Annual Review of Nuclear and Particle Science

Exotic Hadrons at LHCb

Daniel Johnson,[1] Ivan Polyakov,[2] Tomasz Skwarnicki,[3] and Mengzhen Wang[4]

[1]School of Physics and Astronomy, University of Birmingham, Birmingham, United Kingdom; email: daniel.johnson@cern.ch

[2]European Organization for Nuclear Research (CERN), Geneva, Switzerland; email: ivan.polyakov@cern.ch

[3]Department of Physics, Syracuse University, Syracuse, New York, USA; email: tskwarni@syr.edu

[4]Sezione di Milano, Istituto Nazionale di Fisica Nucleare (INFN), Milano, Italy; email: mengzhen.wang@cern.ch

Annu. Rev. Nucl. Part. Sci. 2024. 74:583–612

First published as a Review in Advance on July 9, 2024

The *Annual Review of Nuclear and Particle Science* is online at nucl.annualreviews.org

https://doi.org/10.1146/annurev-nucl-102422-040628

Keywords

hadron spectroscopy, exotic hadrons, tetraquarks, pentaquarks, QCD

Abstract

It has been 5 years since the data sample from the LHCb detector, the first experiment optimized for heavy-flavor physics studies at a hadronic collider, was completed. These data led to many major discoveries in exotic hadron spectroscopy, which we review in this article. We supplement the experimental results with a selection of phenomenological interpretations. As the upgraded LHCb detector is expected to collect a larger data sample starting in 2024, we also discuss the potential of the LHCb program in exotic hadron physics for the near future and beyond.

Contents

1. INTRODUCTION

Hadrons are bound states created by strong interactions, which couple objects that carry a color charge: quarks and gluons. We have known about quarks—elementary fermions with fractional electric charge and one unit of strong color charge—since the mid-1960s when their existence was deduced from the observed mass spectrum of hadrons, which could be explained using three light-quark (q) flavors: up (u; electric charge $+2/3e$), down (d; electric charge $-1/3e$), and strange (s; electric charge $-1/3e$). All hadrons at that time could be explained as bound states either of a quark and an antiquark ($q\bar{q}$) or of three quarks (qqq)—so-called conventional mesons and baryons, respectively. The properties of strong interactions that drove the observed light-hadron mass spectrum were quark flavor independence and the confinement of color charges. Combined with the similarity of the light-quark masses (m_q), flavor independence accounted for the observed isospin symmetry ($m_u \approx m_d$), which, through inclusion of the strange quark ($m_s \approx m_{u,d}$), was extended to $SU(3)_{\text{flavor}}$ symmetry. Confinement limits the extent of unscreened color fields to about the size of a light hadron (~1 fm). When the lightest baryons—that is, nucleons, protons (uud), and neutrons (udd)—are in close proximity, residual strong interactions can bind them into more extended structures known as nuclei [$(qqq)(qqq)\ldots$]. Such nuclear interactions bear some resemblance to the residual electromagnetic interactions through which electrically neutral atoms form molecular structures.

It took another decade to develop a complete theory of strong interactions based on $SU(3)_{\text{color}}$ symmetry—quantum chromodynamics (QCD)—which introduced the gluon (g), a massless elementary boson that mediates color interactions. Unlike the photons of quantum electrodynamics (QED), gluons carry complex color charges—a unit of color and a unit of anticolor. Consequently, gluons could become hadron constituents and form so-called hybrid mesons ($q\bar{q}g$), hybrid baryons ($qqqg$), or glueballs (gg). Going beyond the well-established conventional hadronic states ($q\bar{q}$ and qqq), hybrids are classified as exotic hadrons.

Also falling into the broad category of exotic hadrons are those bound states that comprise more than the minimal number of quarks. Such multiquark states can come in the form of either exotic mesons [e.g., tetraquarks ($qq\bar{q}\bar{q}$)] or exotic baryons [e.g., pentaquarks ($qqqq\bar{q}$)]. In fact, the very first quark model proposals (1) speculated about their existence. QCD provided further motivation for multiquark states since quark or antiquark pairs, $\{qq\}$, in antisymmetric

color combinations act as single antiquarks or quarks. Such pairs could thus become the building blocks of diquark tetraquarks ($\{qq\}\{\overline{q}\overline{q}\}$) or diquark pentaquarks ($\{qq\}\{qq\}\overline{q}$). These hadrons would have compact sizes of the order of the confining scale. Different color schemes of compact multiquark hadrons have been also proposed, like that of so-called hadrocharmonium, in which a light hadron surrounds the heavy charmonium state in the center, both color-polarized [($\{c\overline{c}\}\{q\overline{q}\}$), ($\{c\overline{c}\}\{qqq\}$)]. A further mechanism for the creation of multiquark structures arises if the nuclear type of binding is effective in baryon–meson and meson–meson combinations so as to produce molecular pentaquarks [$(qqq)(q\overline{q})$] or tetraquarks [$(q\overline{q})(q\overline{q})$]. They would be loosely bound and have extended sizes due to two nearly independent confinement volumes. These various quark-binding schemes could lead to different hadron families or to hadrons with mixed features.

Half a century since the formation of QCD, which is considered the exact theory of strong interactions, experimental studies of the hadron spectrum still attract great interest. Because the strong coupling constant becomes large in the confining domain that drives hadronic structures, perturbative methods—so useful in QED applications—are of limited use in QCD. The lattice QCD approach, using numeric methods applied to the QCD Lagrangian, has been very successful in reproducing the observed mass spectrum of stable (i.e., long-lived) conventional hadrons. Numeric simulations of unstable (e.g., excited mesons and baryons) or multiquark structures are in their infancy and are often limited by computational practicalities. Thus, instead of first-principle theoretical predictions, phenomenological models are used to predict the full hadron spectrum, introducing often contradictory assumptions and uncontrollable systematic uncertainties. This leaves many fundamental questions (Do gluons act as hadron constituents? Do compact and/or molecular multiquark hadrons exist? Do they mix with each other and with conventional hadrons? Are diquarks useful concepts for compact hadron substructure?) to be answered experimentally. Therefore, hadron spectroscopy is one of the last frontiers within the Standard Model of interactions still largely driven by experimental studies.

Light-hadron masses are often dominated by quark interaction energy, making their quark content less evident, especially given the presence of three different quark flavors of similar masses. For excited states, this energy can be easily converted into the creation of additional $q\overline{q}$ pairs, which results in large decay widths. Constituent quarks are highly relativistic, making quark-spin-dependent mass splittings large. The masses of charm quarks (c; electric charge $+2/3e$) and beauty quarks (also called bottom quarks) (b; electric charge $-1/3e$) differ substantially and are much larger than their interaction energies, and thus their presence in hadrons is obvious. These heavy quarks are nearly static in hadrons, suppressing their spin-dependent couplings. These large masses lie at the heart of several effective theories, simplifying their theoretical modeling. Furthermore, several states with lower excitation energies are below the threshold for easy hadron disintegration, resulting in narrow widths. These factors together make heavy-quark hadrons particularly important for explorations of various hadronic structures.

The LHCb experiment is the first experiment operating at a hadronic collider to have been optimized for the study of hadrons that contain charm and/or beauty quarks. Large production cross sections at the highest-energy proton–proton collider, combined with the high instantaneous luminosity of the Large Hadron Collider (LHC), provide an unmatched source of charm and beauty quarks that is limited chiefly by the processing capabilities of the detector. The architecture of the LHCb detector is optimized for efficient detection of heavy-quark hadrons with simultaneous suppression of backgrounds arising from the large number of particles produced at the primary pp interaction point. Not surprisingly, the LHCb experiment has produced a large number of discoveries in hadron spectroscopy, which we review in this article.

2. THE LHCb EXPERIMENT

The LHCb experiment was conceived for the study of heavy-flavor hadrons at the LHC—most notably to examine the production and decay of objects containing heavy beauty or charm quarks. The forward geometry of the LHCb detector underscores this objective, instrumenting only regions of high pseudorapidity—between approximately two and five pseudorapidity units—where b and c hadrons are copiously produced and can be detected in a relatively small solid angle, minimizing detector cost. A schematic of the detector is shown in **Figure 1**.

In the endeavor to optimize studies of hadronic spectroscopy, three objectives must be achieved: Misreconstruction effects must be kept to a minimum, the effect of limited experimental resolution must be minimized, and background processes—real and combinatorial—must be suppressed. The characteristics of the LHCb experiment that allow it to satisfy these demands are discussed in this section.

A hallmark of the LHCb detector is its excellent particle identification (PID) performance. For muons, this is achieved through the five stations of its muon system (3) comprising multiwire proportional chambers and gaseous electron multiplier detectors (M1–M5 in **Figure 1**). The system efficiently vetoes hadronic backgrounds and achieves a muon trigger efficiency surpassing 95%, which is of particular importance for those final states that feature a J/ψ meson, as many discussed

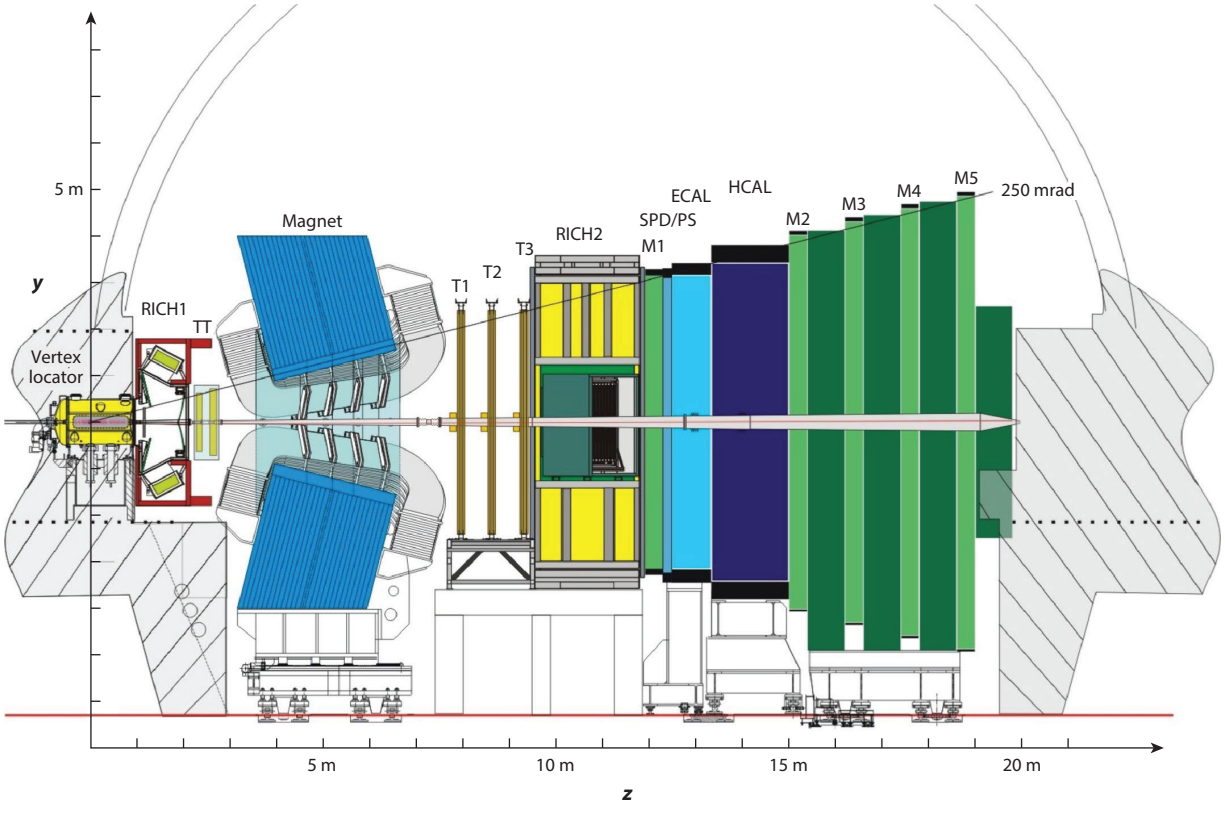

Figure 1

Schematic of the LHCb experiment at CERN. Abbreviations: ECAL, electromagnetic calorimeter; HCAL, hadronic calorimeter; RICH, ring imaging Cherenkov detector; SPD/PS, scintillating pad detector/preshower. Figure adapted from Reference 2 (CC BY 4.0).

in this review do. Useful electron identification capability is delivered by combining information from the hadron and electromagnetic calorimeter systems.

Central to many of the decays used in studies of spectroscopy by the LHCb Collaboration are final states that consist largely or entirely of as many as nine light stable hadrons: pions, kaons, and protons. Without mitigation, the combinatorial background introduced through the misassignation-of-mass hypothesis, in particular for kaons and pions during reconstruction of such high-multiplicity final states, would be very high. This is overcome principally by using two ring imaging Cherenkov (RICH) detectors to collect the Cherenkov radiation emitted as charged particles traverse their radiator volumes; the two RICH detectors accommodate particles in differing momentum ranges. Considering the whole momentum range from 2 to 100 GeV,[1] the efficiency for correctly identifying kaons is found to be approximately 95% with a pion misidentification rate of approximately 10%.

That the best experimental resolution should be targeted is obvious. Its consequences are particularly important for hadron spectroscopy in two areas. First, greater momentum resolution translates directly into better resolution in invariant mass spectra. With improved mass resolution, signals emerge more significantly above broad background shapes, nearby partially reconstructed contributions are more distinctly separated, and clusters of states become more readily resolved (where their natural widths are not limiting), simplifying otherwise complicated fits to overlapping resonances. The performance of the LHCb experiment's tracking system is essential here. It consists of a 55-μm-pitch silicon-strip vertex locator with 104 double-sided modules (one with strips oriented radially, the other azimuthally) arranged at discrete positions along the beam line, surrounding the interaction point, and a further four-layer, 183-μm-pitch silicon-microstrip detector just upstream of the warm dipole magnet (TT). The magnet has a bending power of 4 Tm and is followed by the final three layers of the tracking system (T1–T3). Two technologies are in use in each layer: The innermost region is instrumented once more with 183-μm silicon microstrips, and the outer region, which has lower particle flux, is instrumented with straw tubes. The relative momentum uncertainty for tracks with momentum up to 300 GeV increases from 0.5% below 20 GeV to approximately 0.8% for tracks with momentum of 100 GeV. Through comparison to a range of c and b hadrons whose masses are well known, the systematic uncertainty on the momentum scale is found to be approximately 0.03%. The achieved relative mass resolution is approximately 0.5% up to the $\Upsilon(3S)$ resonance. Such excellent resolution explains, for instance, why fits to backgrounds from $B \to D^{*0}DK$ processes, where a neutral product of the D^{*0} decay was not reconstructed, could be circumvented in the study of $B^{\pm} \to D^{+}D^{-}K^{\pm}$ decays discussed below (see Section 6). The processes were cleanly separated experimentally.

The second consequence of excellent experimental resolution involves the precise determination of impact parameters (IPs). The LHCb experiment relies heavily on the fact that final-state particles produced during the decays of relatively long-lived b and c hadrons—each typically traveling several millimeters in the laboratory frame—exhibit a large IP with respect to the well-measured pp collision point. Many of the online event filters select based on the presence of significantly displaced tracks. Strict IP cuts continue to be employed offline to suppress combinatorial backgrounds formed when "background" particles produced promptly in the pp collision are wrongly included in the reconstruction of a particular decay process. They are especially effective in decays of b particles that involve an intermediate open-charm hadron (D^0 or $D^{\pm}$). The LHCb experiment achieves an IP resolution of approximately 13 μm for the highest-momentum tracks, which deteriorates to approximately 80 μm for the lowest-momentum tracks thanks to the

[1]Throughout this review, the convention $\hbar = c = 1$ is used.

greater role of multiple scattering. Compared to the scale of b and c hadron flight distances, this resolution gives an exceptional opportunity to suppress background from prompt processes.

Despite the low rate of pp interactions per crossing of proton bunches in the LHCb experiment—only a little more than one during Run 1 (2011–2012) and Run 2 (2015–2018)—the abundance of soft hadronic production accompanying the hard scatter of an LHC pp collision allows wide scope for combinatorial backgrounds where particles (mainly pions) are wrongly employed during the reconstruction of a particular process. Requirements regarding the minimum IPs of included particles, enabled by the displaced decays of the original b and c hadrons in most studies of spectroscopy at LHCb, are critical to suppress such backgrounds. They are not universal, however, and significant progress has been made in studies of promptly produced objects that originate at points indistinguishable from the pp collision, including some of those discussed in this review.

A major challenge across the LHCb physics program is the use of decay processes that involve one or more neutral particles; the relatively low efficiency for photon reconstruction and the non-4π acceptance and incomplete reconstruction of the pp interaction products are the primary considerations. Although the reconstruction is challenging, noteworthy efforts have been made to investigate hadron spectroscopy using decays to final states involving neutrals.

The detectors built at the e^+e^- B factories, most recently Belle II, also have excellent heavy-hadron reconstruction efficiencies, which can even surpass the LHCb capabilities, especially for high-multiplicity final states, final states with photons, or those that involve $K^0_s \to \pi^=\pi^-$ decays. However, the significance of the LHCb experiment lies in its achievement of good heavy-hadron detection at a high-energy hadron–hadron collider. The strong production cross sections provide an overwhelming competitive advantage over the electromagnetic processes. Furthermore, b baryons, which are unreachable at the B factories, are copiously produced at the LHC together with b mesons, providing additional avenues for exotic hadron studies.

3. THE $\chi_{c1}(3872)$ STATE

The beginning of experimental results on exotic heavy-quark spectroscopy dates two decades back to when the narrow $\chi_{c1}(3872)$ state was discovered in $B^{+,0} \to \chi_{c1}(3872)K^{+,0}$ (charge conjugate states are implied), $\chi_{c1}(3872) \to \pi^+\pi^- J/\psi$, $J/\psi \to \ell^+\ell^-$ decays by the Belle $e^+e^- \to B\overline{B}$ experiment (4). Just 36 ± 7 signal events were observed in the data sample corresponding to an integrated luminosity of about 140 fb^{-1}. The observation was later confirmed by the BaBar experiment (5), and by inclusive studies dominated by the prompt production at the $p\bar{p}$ Tevatron collider, by the CDF (730 ± 90 signal events in 0.22 fb^{-1} of data) (6), and by the D0 (7) experiments. The state was intriguing since its mass coincided exactly with the threshold for $D^0\overline{D}^{*0}$ decays. As if to underline the advantages of a high-energy pp collider for studies of hadronic spectroscopy, it took a dataset that initially corresponded to an integrated luminosity of just 0.035 fb^{-1} for the LHCb Collaboration to observe promptly produced 565 ± 62 $\chi_{c1}(3872)$ events at the LHC (8). The ease of $\chi_{c1}(3872)$ detection at LHCb reflects not only the increased heavy-quark cross section at the higher beam collision energies ($\sqrt{s} = 7$–13 TeV at the LHC versus 2 TeV at the Tevatron) but also (and much more so) the higher detection efficiency of the forward LHCb detector compared to that of the central detectors, which were optimized for high-transverse-momentum physics rather than heavy-flavor studies.

Settling the $\chi_{c1}(3872)$ quantum numbers was an early and important contribution of the LHCb experiment. Previously, the CDF experiment had narrowed them down to $J^{PC} = 1^{++}$ or 2^{-+} in the sample of $2,292 \pm 113$ $\chi_{c1}(3872)$ events (0.78 fb^{-1}) (9). The sensitivity was limited by high backgrounds and the lack of $\chi_{c1}(3872)$ polarization in the inclusive studies. The Belle

experiment—with 173 ± 16 signal events reconstructed in B decays (711 fb^{-1}), which allowed for the $\chi_{c1}(3872)$ polarization and small backgrounds—agreed with this J^{PC} selection (10). With a 2011 dataset corresponding to an integrated luminosity of 1 fb^{-1}, the LHCb Collaboration reconstructed 313 ± 26 signal events in B meson decays with a background level comparable to that of the e^+e^- experiments thanks to the excellent B-decay vertex separation from the primary pp interaction point (11). By performing a full five-dimensional angular analysis for the first time, it was possible to favor overwhelmingly the 1^{++} assignment over 2^{-+}. Like the previous analyses, it was assumed that the $\chi_{c1}(3872) \to (\pi^+\pi^-)J/\psi$ decay proceeds via S-wave. With the 2011–2012 dataset (3 fb^{-1}) and 1,011 ± 38 signal events, the LHCb Collaboration found no evidence for D-wave contributions, setting an upper limit of <4% at a 95% CL on their fraction, and firmly established $J^{PC} = 1^{++}$ as opposed to all other alternatives (12).

Such quantum numbers are consistent with the $D^0\bar{D}^{*0}$ molecular interpretation and compact tetraquark models as well as the conventional $\chi_c(2\,^3\mathrm{P}_1)$ meson hypothesis. However, the $\chi_{c1}(3872)$ state cannot be a pure charmonium state, which is best evidenced by the LHCb analysis of the dipion mass spectrum in $\chi_{c1}(3872) \to \pi^+\pi^- J/\psi$ decays performed with the 2011–2018 data sample (9 fb^{-1}) and 6,788 ± 117 signal events reconstructed in $B^+ \to \chi_{c1}(3872)K^+$ decays (13). The decay is dominated by the isospin-violating $\chi_{c1}(3872) \to \rho^0 J/\psi$ decay with the isospin-conserving $\chi_{c1}(3872) \to \omega J/\psi$ decay contributing significantly $(21.4 \pm 2.3 \pm 2.0)\%$, strongly amplified by ρ^0-ω interference. From this, the LHCb Collaboration determined the ratio of coupling constants, $g_{\chi_{c1}(3872)\to\rho^0 J/\psi}/g_{\chi_{c1}(3872)\to\omega J/\psi} = 0.29 \pm 0.04$, which is an order of magnitude larger than the amount of isopin violation determined for the pure $c\bar{c}$ state, $g_{\psi(2S)\to\pi^0 J/\psi}/g_{\psi(2S)\to\eta J/\psi} = 0.045 \pm 0.001$ (13). Large isospin violation is naturally expected in models in which the $\chi_{c1}(3872)$ state has a significant $D\bar{D}^*$ component, either as constituents (i.e., in the molecular model) or generated dynamically in the decay (14). The proximity of the $\chi_{c1}(3872)$ mass to the $D^0\bar{D}^{*0}$ threshold enhances such contributions over D^+D^{*-} combinations, which are 8 MeV heavier. It has also been suggested in compact tetraquark models that two neutral states, which are expected in the diquark model, could be degenerate and mix to form the $\chi_{c1}(3872)$ state, giving rise to large isospin violation in $\chi_{c1}(3872)$ decays (15).

The large number of reconstructed $\chi_{c1}(3872) \to \pi^+\pi^- J/\psi$ decays coming from the displaced b hadron vertex allowed the LHCb Collaboration to achieve the best sensitivity in seeking to measure the $\chi_{c1}(3872)$ mass and width. Two complementary approaches were taken: exclusive $B^+ \to \chi_{c1}(3872)K^+$ reconstruction (16), which gives the best background suppression; and semi-inclusive $\chi_{c1}(3872)$ reconstruction with a displaced vertex, which integrates over all b hadron species (17), yielding more signal (15,630 ± 380 events in a dataset corresponding to an integrated luminosity of 3 fb^{-1}) but also resulting in a higher background level. The mass determinations are consistent with those made previously and are the most precise to date (18). The measured mass is still indistinguishable from the $D^0\bar{D}^{*0}$ threshold. The width determinations, according to a Breit–Wigner parameterization, yielded values different from zero for the first time (combined: 1.19 ± 0.21 MeV) (18). However, this parameterization has questionable value for a state coinciding with a coupled-channel threshold. Therefore, the LHCb Collaboration also undertook an analysis using a Flatté-like parameterization that contains parameters for the couplings to the analyzed $\pi^+\pi^- J/\psi$ channel as well as to the $D^0\bar{D}^{*0}$ and $D^+\bar{D}^{*-}$ thresholds and with the $\pi^+\pi^-\pi^0 J/\psi$ channel constrained to the measurements made by the other experiments. The pole mass, the couplings to the $\pi^+\pi^- J/\psi$ and $D\bar{D}^*$ channels (the latter assumed to be isospin symmetric), and the Γ_0 parameter to catch all other contributions were free parameters when fitting the observed $\pi^+\pi^- J/\psi$ mass distributions. The obtained underlying line shape is much narrower (FWHM = 0.22 ± 0.07 MeV; statistical error only) than the Breit–Wigner line shape.

However, the fit quality is only marginally improved, reflecting difficulty in probing the line shape when the detector mass resolution dominates over the line-shape effects by a large factor. The pole position, and therefore the binding energy, is poorly constrained because of its strong correlation to the other fit parameters. Furthermore, the obtained value of $\Gamma_0 = 1.4 \pm 0.4$ MeV was uncomfortably large, pointing to the importance of modes not explicitly represented in the line-shape model. In the future, increased statistics and including in the analysis other invariant mass distributions (alongside that of the $\pi^+\pi^- J/\psi$ candidates) in a simultaneous coupled-channel fit will improve LHCb's sensitivity to the $\chi_{c1}(3872)$ mass and width parameters.

Decays of the $\chi_{c1}(3872)$ state to a J/ψ or $\psi(2S)$ meson and a photon provide a valuable opportunity to understand its nature. The partial widths of these decays depend on the overlap of the $c\bar{c}$ wave function in the $\chi_{c1}(3872)$ state with that in the charmonium state. Therefore, the ratio of the corresponding branching fractions, $R_{\psi\gamma} \equiv \mathcal{B}(\chi_{c1}(3872) \to \psi(2S)\gamma)/\mathcal{B}(\chi_{c1}(3872) \to J/\psi\gamma)$, should depend heavily on whether the $\chi_{c1}(3872)$ state has $D\overline{D}^*$ molecule or charmonium components.

The BaBar Collaboration has reported evidence for the $\chi_{c1}(3872) \to \psi(2S)\gamma$ decay and measured $R_{\psi\gamma} = 3.4 \pm 1.4$ (19). In contrast, the Belle Collaboration found no significant $\chi_{c1}(3872) \to \psi(2S)\gamma$ signal and reported an upper limit of $R_{\psi\gamma} < 2.1$ (90% CL) (20). Using a data sample corresponding to an integrated luminosity of 3 fb^{-1}, collected during 2011 and 2012, the LHCb Collaboration obtained evidence for the $\chi_{c1}(3872) \to \psi(2S)\gamma$ decay in a sample of $B^+ \to \chi_{c1}(3872)K^+$ decays with a yield of 36.4 ± 9.0 candidates and a significance of 4.4 standard deviations (see **Figure 2**). The ratio $R_{\psi\gamma}$ was measured to be $2.46 \pm 0.64 \pm 0.29$ (21), which is compatible with both preceding measurements by the BaBar and Belle Collaborations. The measured value exceeds estimates of $\mathcal{O}(10^{-3})$ for the $\chi_{c1}(3872)$ state as a pure $D\overline{D}^*$ molecular state (22–24), thus indicating the presence of a charmonium component. However, it is not in conflict with a predominantly molecular nature for the $\chi_{c1}(3872)$ state (25) and can be explained with only a 5–12% admixture of charmonium (23) or even less (26).

In a more recent analysis by the BESIII Collaboration, no signal of the decay $\chi_{c1}(3872) \to \psi(2S)\gamma$ was found, and an upper limit on $R_{\psi\gamma}$ was set at 0.59 (90% CL) (27). This result is in tension with the measurements by the LHCb and BaBar Collaborations. A future analysis from the LHCb Collaboration, incorporating the larger Run 2 dataset, will elucidate it.

To study $\chi_{c1}(3872)$ production in decays of various b hadrons, the $\chi_{c1}(3872) \to \pi^+\pi^- J/\psi$ decay mode was used. In addition to the well-established $B^+ \to \chi_{c1}(3872)K^+$ (16) decay, the new decays $B_s^0 \to \chi_{c1}(3872)K^+K^-$ (28), $B_s^0 \to \chi_{c1}(3872)\pi^+\pi^-$ (29), and $\Lambda_b^0 \to \chi_{c1}(3872)pK^-$ (30) were observed for the first time (see **Figure 2**). It was found that $(38.9 \pm 4.9)\%$ of $B_s^0 \to \chi_{c1}(3872)K^+K^-$ decays and $(58 \pm 15)\%$ of $\Lambda_b^0 \to \chi_{c1}(3872)pK^-$ decays proceed via the ϕ and $\Lambda(1520)$ intermediate resonances, respectively. The $B_s^0 \to \chi_{c1}(3872)\pi^+\pi^-$ decay was found to be dominated by $f_0(980)$ and $f_0(1500)$ resonance components. Branching fractions of these decay modes relative to those in analogous decays, replacing the $\chi_{c1}(3872)$ candidate with a conventional $\psi(2S)$ $c\bar{c}$ state, including the subsequent $X \to \pi^+\pi^- J/\psi$ decay, were measured to be

$$\mathcal{R}_{B^+\to XK^+} = (3.69 \pm 0.07 \pm 0.06) \times 10^{-2}, \qquad \mathcal{R}_{\Lambda_b^0\to Xp K^-} = (5.4 \pm 1.1 \pm 0.2) \times 10^{-2},$$

$$\mathcal{R}_{B_s^0\to X\phi} = (2.42 \pm 0.23 \pm 0.07) \times 10^{-2}, \quad \text{and} \quad \mathcal{R}_{B_s^0\to X\pi^+\pi^-} = (6.8 \pm 1.1 \pm 0.2) \times 10^{-2},$$

where $\mathcal{R}_{B\to XY}$ represents the corresponding ratio of branching fractions $\mathcal{B}(B \to \chi_{c1}(3872)Y)/\mathcal{B}(B \to \psi(2S)Y)$. The ratio for $B_s^0 \to X\phi$ decays is consistent with, but more precise than, the value of $(2.21 \pm 0.29 \pm 0.17) \times 10^{-2}$ reported previously by the CMS Collaboration (31). The large variation of the $\mathcal{R}$ ratio between production modes may reflect a tetraquark component in the $\chi_{c1}(3872)$ state (32).

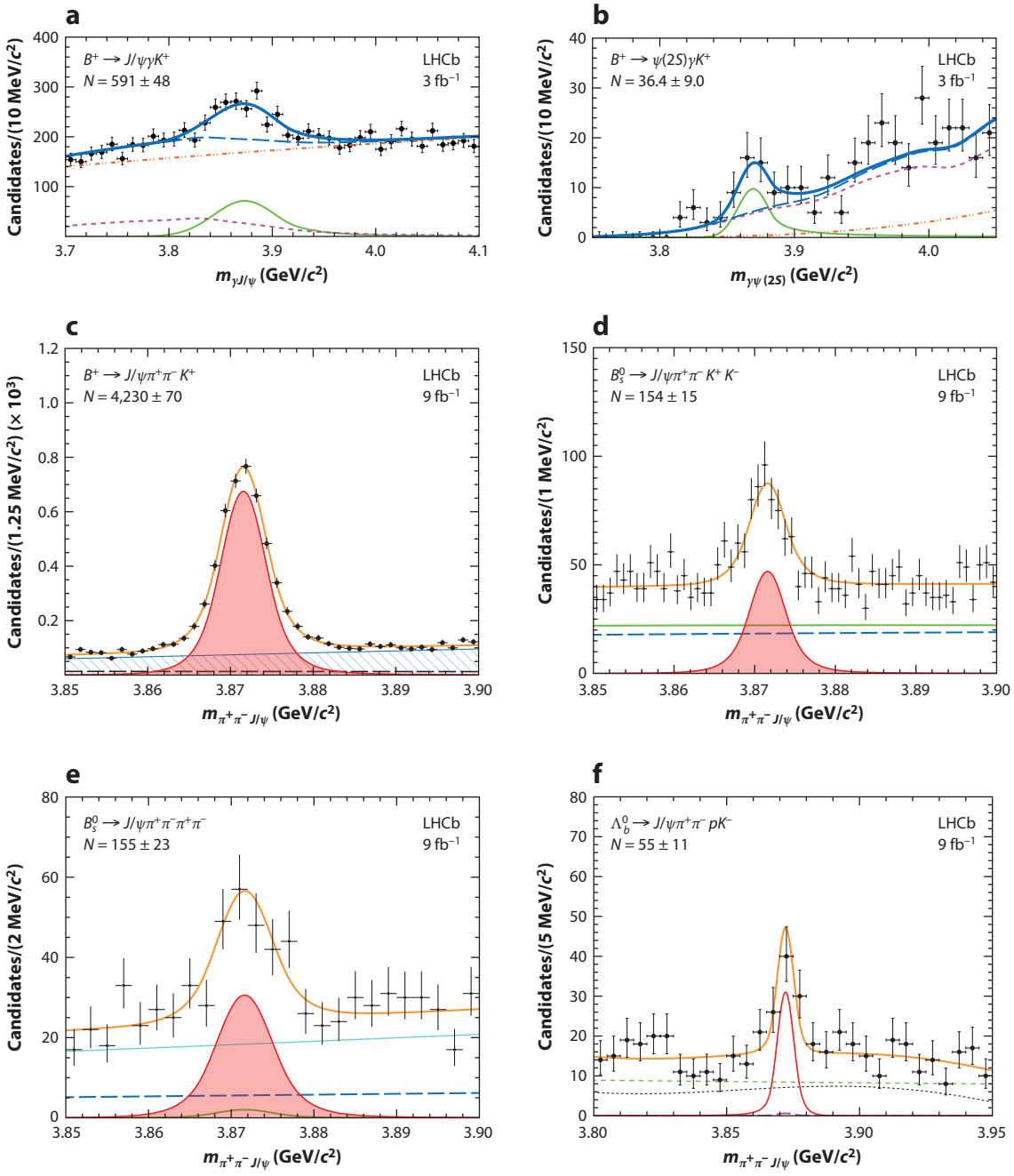

Figure 2

The $\chi_{c1}(3872)$ signal in various b hadron decays with corresponding yields: (*a*) $B^+ \to \chi_{c1}(3872)_{J/\psi\gamma}K^+$, (*b*) $B^+ \to \chi_{c1}(3872)_{\psi(2S)\gamma}K^+$, (*c*) $B^+ \to \chi_{c1}(3872)_{J/\psi\pi^+\pi^-}K^+$, (*d*) $B_s^0 \to \chi_{c1}(3872)_{J/\psi\pi^+\pi^-}K^+K^-$, (*e*) $B_s^0 \to \chi_{c1}(3872)_{J/\psi\pi^+\pi^-}\pi^+\pi^-$, and (*f*) $\Lambda_b^0 \to \chi_{c1}(3872)_{J/\psi\pi^+\pi^-}pK^-$. In panels *a* and *b*, the signal is represented by the solid green lines; in panels *c*, *d*, and *e*, the signal is represented by the shaded red areas; and in panel *f*, the signal is represented by the solid red line. Panels *a* and *b* adapted from Reference 21 (CC BY 4.0). Panel *c* adapted from Reference 16 (CC BY 4.0). Panel *d* adapted from Reference 28 (CC BY 4.0). Panel *e* adapted from Reference 29 (CC BY 4.0). Panel *f* adapted from Reference 30 (CC BY 4.0).

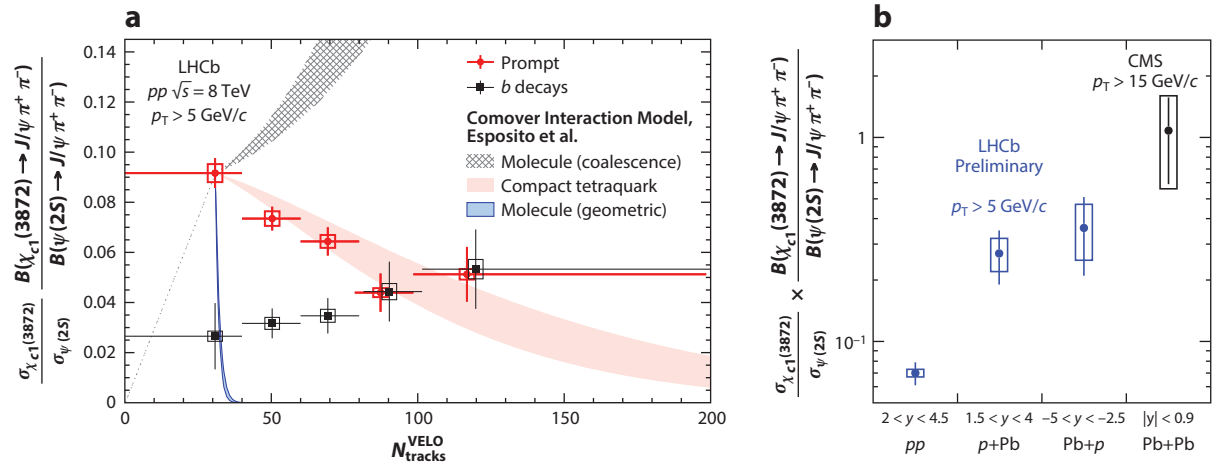

Figure 3

Ratio of $\chi_{c1}(3872)$ and $\psi(2S)$ cross sections multiplied by branching fractions of decay to $J/\psi\pi^+\pi^-$ states in (*a*) *pp* collisions depending on event multiplicity (34) [compared to the theoretical models from Esposito et al. (35)] and (*b*) *pp*, *p*+Pb, Pb+*p*, and Pb+Pb collisions (37). Panel *a* adapted from Reference 34 (CC BY 4.0). Panel *b* adapted from Reference 37 (CC BY 4.0).

Just as for *b* decays, the $\chi_{c1}(3872)$ prompt production cross section was measured relative to that of the $\psi(2S)$ meson using the $\pi^+\pi^- J/\psi$ decay mode. In *pp* collisions at $\sqrt{s} = 7$ TeV, the product of the $\chi_{c1}(3872)$ production cross section and the branching ratio into $\pi^+\pi^- J/\psi$ was measured for $\chi_{c1}(3872)$ candidates with rapidity between 2.5 and 4.5 and transverse momentum between 5 and 20 GeV (both promptly and via *b* decays). It was found to be $5.4 \pm 1.3 \pm 0.8$ nb (8). In an analysis of *pp* collisions at $\sqrt{s} = 8$ and 13 TeV, the double-differential cross sections of the $\chi_{c1}(3872)$ state relative to that of the $\psi(2S)$ meson were measured as a function of transverse momentum (p_T) and rapidity (y) separately for promptly produced $\chi_{c1}(3872)$ hadrons and those from *b* decays (33). The ratios, integrated over the kinematic region $4 < p_T < 20$ GeV and $2.0 < y < 4.5$, were as follows:

$$R^{8\,\text{TeV}}_{\text{prompt}} = (7.6 \pm 0.5 \pm 0.9) \times 10^{-2}, \qquad R^{8\,\text{TeV}}_{\text{nonprompt}} = (4.6 \pm 0.4 \pm 0.5) \times 10^{-2},$$

$$R^{13\,\text{TeV}}_{\text{prompt}} = (7.6 \pm 0.3 \pm 0.6) \times 10^{-2}, \quad \text{and} \quad R^{13\,\text{TeV}}_{\text{nonprompt}} = (4.4 \pm 0.2 \pm 0.4) \times 10^{-2}.$$

In *pp* collisions at $\sqrt{s} = 8$ TeV, the production of $\chi_{c1}(3872)$ and $\psi(2S)$ particles was also studied as a function of charged particle multiplicity (34) (see **Figure 3**). Prompt production of the $\chi_{c1}(3872)$ relative to the $\psi(2S)$ particles was found to decrease with event multiplicity while, for $\chi_{c1}(3872)$ and $\psi(2S)$ particles produced via *b* decays, no significant dependence on multiplicity was found, as expected for production at the isolated secondary vertex. Possible explanations involve breakup of the $\chi_{c1}(3872)$ particle, extended in size by its tetraquark component, by rescattering with comoving partons. However, the exact interpretation is still unclear (35, 36).

For the first time, $\chi_{c1}(3872)$ production was measured in *p*+Pb collisions at $\sqrt{s_{NN}} = 8.16$ TeV in both forward ($1.5 < y < 4$, *p*+Pb) and backward ($-5 < y < -2.5$, Pb+*p*) rapidity regions (37). Measurements of cross sections multiplied by the branching fraction of decay to $J/\psi\pi^+\pi^-$ states relative to that of the $\psi(2S)$ state yield the following ratios:

$$R^{p+\text{Pb}} = 0.27 \pm 0.08 \pm 0.05 \quad \text{and} \quad R^{\text{Pb}+p} = 0.36 \pm 0.15 \pm 0.11.$$

These are an order of magnitude larger than in *pp* collisions and closer to the value of $1.08 \pm 0.49 \pm 0.52$ measured by the CMS Collaboration in Pb+Pb collisions at significantly higher

transverse momentum (38). In this ratio, effects from modification of the nuclear parton distribution function largely cancel. Given that in pp collisions this ratio decreases with multiplicity, one may suggest that as the collision system size—or density—increases, the $\chi_{c1}(3872)$ production becomes dominated by a new mechanism, such as quark coalescence (37). However, the experimental errors in all the heavy-ion collision results are very large. More data are needed before these effects can be clearly established.

4. PENTAQUARK STATES

Multiquark states that consist of four quarks and one antiquark have been predicted since the inception of the quark model, and decades of efforts have been made to search for these pentaquarks experimentally. Over the first 50 years, candidates came and went, but none were widely accepted. Some of these states had both exotic and conventional interpretations and are the subject of continuing debate, such as the $\Lambda(1405)$ particle, which can be thought of as either a $\overline{K}N$ bound state or a conventional baryon with mass shifted due to the couplings to virtual channels (39). Others were not confirmed in subsequent experiments with improved statistical precision. One classic example is the $\Theta(1540)^+$ particle (40–42).

During the past decade, the LHCb Collaboration has reported observations and evidence of several pentaquark candidates that are charmonium-like, containing a $c\bar{c}$ pair. Various exclusive b hadron decays were studied, and intermediate states emerged in strong decays to a charmonium meson and a light baryon (43–47). Their decay signatures indicate minimal quark content—a $c\bar{c}$ quark pair and three light quarks—placing them firmly outside the household of conventional baryons.

4.1. Pentaquark Candidates in Beauty Baryon Decays

The first observation of charmonium-like pentaquark candidates originated in a study of the $\Lambda_b^0 \to J/\psi p K^-$ decay. Using a data sample corresponding to an integrated luminosity of 3 fb^{-1}, the LHCb Collaboration reported the observation of two $J/\psi p$ states ($c\bar{c}uud$) in an amplitude analysis (43). One of these states, referred to as $P_c(4450)^+$, has a mass of approximately 4,450 MeV. It contributes an obvious peaking structure in the $J/\psi p$ invariant mass spectrum with a width too narrow to be explained by reflections from conventional $\Lambda^*(\to pK^-)$ resonances (48). The other broad $P_c(4380)^+$ state (width of about 200 MeV) was not directly visible in the $J/\psi p$ mass spectrum but was needed in the amplitude model to reach a good description of the multidimensional dataset. As this amplitude model is now obsolete (44, 49), the question of whether broad pentaquark states are needed for a good description of these data remains.

By adding data collected by the LHCb Collaboration between 2015 and 2018 at a higher pp collision energy, with a total integrated luminosity of 6 fb^{-1}, and with a further improvement in the event selection, a ninefold increase of the sample size was reached in the reanalysis of $\Lambda_b^0 \to J/\psi p K^-$ decays (44). A one-dimensional $J/\psi p$ mass spectrum analysis was performed. With the improved statistical precision, the $J/\psi p$ structure at 4,450 MeV was found to be composed of two narrower peaks close to one another, and a new peaking state at 4,312 MeV was also uncovered (see **Figure 4**). Masses, widths, and relative fractions of these new narrow peaking states are listed in **Table 1**. The $P_c(4312)^+$ state lies right below the mass threshold of the $\Sigma_c\bar{D}$ baryon–meson combination and has a statistical significance of 7.3σ. The overlapping narrow states $P_c(4440)^+$ and $P_c(4457)^+$ are close to the mass threshold of the $\Sigma_c\bar{D}^*$ combination, and the statistical significance of the two-peak hypothesis against the $P_c(4450)^+$ single-peak hypothesis is 5.4σ.

The narrow widths of the $P_c(4312)^+$, $P_c(4440)^+$, and $P_c(4457)^+$ states, despite their large decay phase space, call for a decay width suppression mechanism. In the tightly bound multiquark

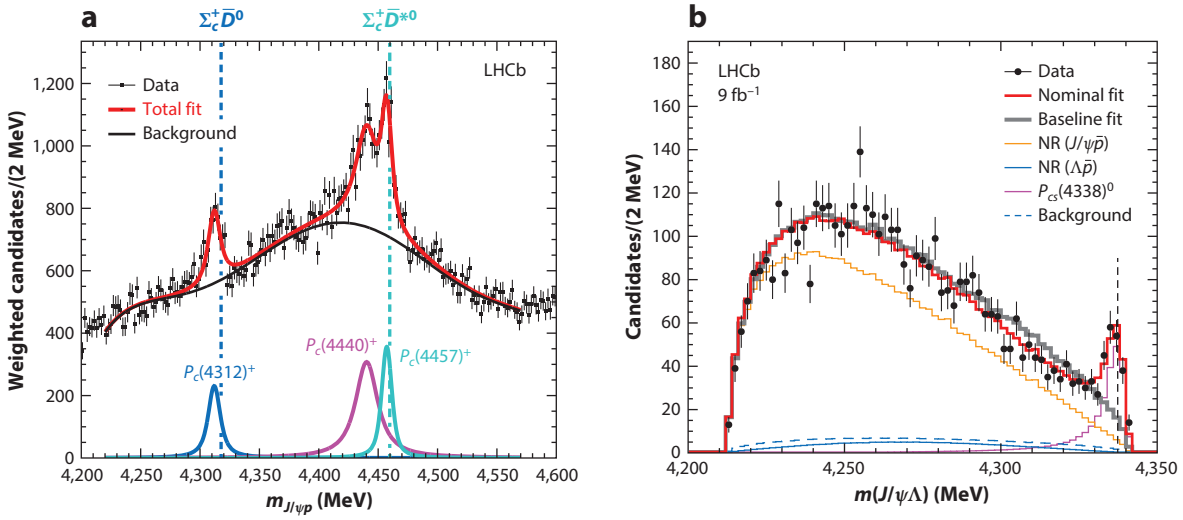

Figure 4

Pentaquark candidates observed by the LHCb Collaboration. (*a*) The peaking states $P_c(4312)^+$, $P_c(4440)^+$, and $P_c(4457)^+$ observed in a $J/\psi\, p$ mass spectrum analysis of the $\Lambda_b^0 \to J/\psi\, pK^-$ data sample. Black dots with error bars show the data distribution, where single-event weights are applied to suppress the contribution from the conventional Λ^* components. Peaking positions of these P_c states are close to the mass thresholds of $\Sigma_c^+\bar{D}^{(*)0}$ combinations (*vertical dashed lines*). Panel adapted from Reference 44 (CC BY 4.0). (*b*) The $J/\psi\,\Lambda$ mass projection of the $B^- \to J/\psi\,\Lambda\bar{p}$ amplitude analysis in which the pentaquark candidate $P_{cs}(4338)^0$ was observed. The $P_{cs}(4338)^0$ peaking position is close to the mass threshold of the $\Xi_c^+ D^-$ combination (*vertical black dashed line*). Panel adapted from Reference 47 (CC BY 4.0). Abbreviation: NR, nonresonant.

model, it is questionable whether a potential barrier, such as an angular momentum barrier (50), can provide enough spatial separation between the charm quarks and antiquarks for effective width suppression. The loosely bound meson–baryon molecular model provides a more natural interpretation of these narrow structures because the charm quarks and antiquarks are separated by much larger distances, making it harder for them to recombine to form the J/ψ meson. The binding energy of hadronic molecules cannot be large; it is usually predicted to be at the $\mathcal{O}$(10MeV) level (51) on par with nucleon binding; thus, their masses are expected to be near the mass thresholds of the meson–baryon combinations, which would be consistent with the observed P_c peak positions. The observed mass splitting between the $P_c(4312)$ and the other two narrow P_c states cannot be reproduced with comparable precision in the compact pentaquark model when attributed to the difference between quark orbital angular momenta (50). The existence of $\Sigma_c\bar{D}^{(*)}$ hadronic molecules was predicted (52–55) before the first pentaquark observation (43) and continues to be the most popular theoretical interpretation (51, 56–76). It was suggested that a triangle singularity could generate near-threshold peaks in the $J/\psi\, p$ mass spectrum (77–80), but the LHCb experiment

Table 1 Masses and widths of narrow pentaquarks observed by the LHCb Collaboration in the $\Lambda_b^0 \to J/\psi\, pK^-$ data sample (44)

State	Mass (MeV)	Width (MeV)	Relative fraction (%)
$P_c(4312)^+$	$4{,}311.9 \pm 0.7^{+6.8}_{-0.6}$	$9.8 \pm 2.7^{+3.7}_{-4.5}$	$0.30 \pm 0.07^{+0.34}_{-0.09}$
$P_c(4440)^+$	$4{,}440.3 \pm 1.3^{+4.1}_{-4.7}$	$20.6 \pm 4.9^{+8.7}_{-10.1}$	$1.11 \pm 0.33^{+0.22}_{-0.10}$
$P_c(4457)^+$	$4{,}457.3 \pm 0.6^{+4.1}_{-1.7}$	$6.4 \pm 2.0^{+5.7}_{-1.9}$	$0.53 \pm 0.16^{+0.15}_{-0.13}$

has demonstrated that the observed peaks are too narrow to be explained in that way (see the supplemental material of Reference 44). The hadrocharmonium model can accommodate $P_c(4440)^+$ and $P_c(4457)^+$ as quasi-$\psi(2S)p$ states and $P_c(4312)^+$ as a quasi-$\chi_{c0}p$ state (81). When taking this hypothesis as input to fix its free parameters, seven more states are predicted in the same mass range [quasi-$\eta_c(2S)p$, quasi-$\chi_{c1}p$, quasi-h_cp, and quasi-$\chi_{c2}p$ states], which have not been observed.

A multidimensional amplitude analysis of $\Lambda_b^0 \to J/\psi pK^-$ decays using the combined LHCb Run 1 and 2 datasets has not been published. Such an analysis could provide additional inputs for understanding the nature of these P_c states by measuring their spin-parity quantum numbers and investigating the possible contributions from broad $J/\psi p$ states. The helicity amplitude formulation used in Reference 43 was later corrected to properly align proton helicities from conventional (pK^-) and exotic ($J/\psi p$) hadron contributions (49). Some of the ongoing efforts of the amplitude analysis are documented in Reference 82, where several outstanding challenges have been identified. The huge data sample and complicated multidimensional fit function with a large number of free parameters require the use of high-speed processors (e.g., GPUs) to perform the amplitude fits within a reasonable time frame. The small relative production fractions for the narrow P_c states in $\Lambda_b^0 \to J/\psi pK^-$ decays (summarized in **Table 1**) result in a low tolerance for mismodeling of the rest of the components contributing to the decay amplitude. Better external inputs concerning the properties of conventional hadrons (Λ excitations) contributing to the Λ_b^0 decay would be helpful, especially in the poorly known high pK^- high-mass region. Potential $\Sigma_c^{(*)}\bar{D}^{(*)}$ coupled-channel effects can have a significant impact on the interpretation of the properties of P_c states (82). A joint analysis of $\Lambda_b^0 \to J/\psi pK^-$ and $\Lambda_b^0 \to \Sigma_c^{(*)}\bar{D}^{(*)}K^-$ data using a coupled-channel line-shape model will be useful alongside the data collected with the upgraded LHCb detector.

Triggered by the pentaquark-candidate observations made in the $\Lambda_b^0 \to J/\psi pK^-$ decay (43), two additional amplitude analyses were performed to search for pentaquarks in similar b baryon decays. In 2016, the LHCb Collaboration released the amplitude analysis result of the Cabibbo-suppressed decay $\Lambda_b^0 \to J/\psi p\pi^-$ using data collected in 2011 and 2012, which supported the existence of pentaquark candidates contributing to the $J/\psi p$ system (83). Using the larger pp dataset collected between 2011 and 2018, corresponding to an integrated luminosity of 9 fb^{-1}, an amplitude analysis of approximately 1,750 $\Xi_b^- \to J/\psi\Lambda K^-$ decays was carried out, and evidence was found for a $P_{cs}(4459)^0$ particle decaying to a $J/\psi\Lambda$ final state. Based on a relativistic Breit–Wigner line-shape description, its mass and width were measured to be $4{,}458.8 \pm 2.9^{+4.7}_{-1.1}$ MeV and $17.3 \pm 6.5^{+8.0}_{-5.7}$ MeV, respectively, behaving as a narrow peaking state just below the mass threshold of the $\Xi_c^0 D^{*0}$ combination. Inspired by the observation of the $P_c(4440)^+$ and $P_c(4457)^+$ states close to the $\Sigma_c\bar{D}^*$ mass threshold, the two-peak hypothesis of the $P_{cs}(4459)^0$ particle was tested, but it could be neither confirmed nor rejected using the current dataset.

4.2. Pentaquark Candidates in Beauty Meson Decays

Decays of B mesons to $J/\psi p$ or $J/\psi\Lambda$ particles and an additional light-flavor baryon offer a unique environment to precisely study properties of hidden-charm pentaquark candidates. These decays benefit from smaller contributions from light-flavor conventional resonances decaying into baryon–baryon final states compared to the situations of the $\Lambda_b^0 \to J/\psi pK^-$ (44) and $\Xi_b^- \to J/\psi\Lambda K^-$ (45) decays, whose amplitudes are dominated by conventional resonances in pK^- and ΛK^- systems. In 2019, the LHCb Collaboration reported the first observation of the decay $B_s^0 \to J/\psi p\bar{p}$ (84) using a pp dataset corresponding to an integrated luminosity of 5.2 fb^{-1}. An enhancement of its measured branching fraction compared to the predicted value (85) hinted at unexpected exotic resonances contributing to this decay channel. The intermediate structures in the $B_s^0 \to J/\psi p\bar{p}$ decay were investigated using the LHCb data collected between 2011 and 2018

corresponding to an integrated luminosity of 9 fb^{-1} (46). An excess at about 4.3 GeV was seen in the $J/\psi\, p$ invariant mass spectrum, indicating the potential contributions of pentaquark candidates. An amplitude analysis was performed to extract the properties of the possible state and showed evidence for a $J/\psi\, p$ structure, denoted as $P_c(4337)^+$, with a mass and width of $4{,}337^{+7}_{-4} \pm 2$ and $29^{+26}_{-12} \pm 14$ MeV, respectively (46). The significance of the new state is 3.1σ; as such, more data are needed to verify the existence of this state. The contribution from the $P_c(4312)^+$ state to the $B_s^0 \to J/\psi\, p\bar{p}$ decay was also tested, and no evidence was found.

The latest observation of a hidden-charm pentaquark candidate was found in the $B^- \to J/\psi\, \Lambda \bar{p}$ (47) decay. An amplitude analysis was applied to a sample of $B^- \to J/\psi\, \Lambda \bar{p}$ decays using a helicity-based formalism optimized for analyzing three-body decays (86). Observation of a $J/\psi\, \Lambda$ intermediate structure was reported with a statistical significance higher than 15σ. This ($c\bar{c}sud$) pentaquark candidate, denoted by $P_{cs}(4338)^0$, was measured to have a Breit–Wigner mass of $4{,}338.2 \pm 0.7 \pm 0.4$ MeV and a width of $7.0 \pm 1.2 \pm 1.3$ MeV. The amplitude analysis favored a $J^P = 1/2^-$ assignment. The hypothesis of $J = 1/2$ was established and the $J^P = 1/2^+$ assignment was excluded with 90% confidence. Its mass—right at the $\Xi_c \bar{D}$ threshold—and narrow width of $7.0 \pm 1.2 \pm 1.3$ MeV, along with its $J^P = 1/2^-$ spin-parity, support a molecular interpretation. This makes the $P_{cs}(4338)^0$ state a likely $\Xi_c^0 \bar{D}^0$ analog of the P_c^+ state in the $\Sigma_c^0 \bar{D}^0$ system. Furthermore, as for the $P_{cs}(4459)^0$ case, a $\Xi_c' \bar{D}$ state is expected, and a total of three additional strange pentaquarks is therefore predicted (87).

5. HIDDEN-CHARM TETRAQUARK CANDIDATES

One of the earliest heavy-quark tetraquark candidates was the $Z_c(4430)^+$ state in its decay to the $\psi(2S)\pi^+$ final state, from a study of approximately 2,000 $\bar{B}^0 \to \psi(2S)\pi^+ K^-$ decays by the Belle Collaboration (88). It was the first explicitly exotic tetraquark structure, but the road to its confirmation at e^+e^- machines was not always smooth (89). The LHCb experiment reconstructed 25,000 of the B decays in a dataset corresponding to an integrated luminosity of 3 fb^{-1}. By means of a four-dimensional amplitude analysis, they confirmed significant resonant activity with a spin-parity of $J^P = 1^+$ in the $\psi(2S)\pi^+$ channel in the mass region of interest (90). The result was consistent with the amplitude analysis results from the Belle experiment (91). When interpreted as one Breit–Wigner resonance, the $Z_c(4430)^+$ mass and width are $4{,}478 \pm 18$ and 181 ± 31 MeV, respectively (18). The LHCb analysis also indicated a significant structure in the 0^- or 1^+ $\psi(2S)\pi^+$ wave at lower mass. The Belle experiment analyzed 32,000 $\bar{B}^0 \to J/\psi\, \pi^+ K^-$ decays and claimed a significant, and very broad ($370 \pm 70^{+70}_{-132}$ MeV), 1^+ $Z_c(4200)^+$ resonance in the amplitude model in addition to the $Z_c(4430)^+$ resonance, which had been included with fixed mass and width (92). The LHCb experiment also demonstrated, with high confidence, the presence of exotic hadron structures in $\bar{B}^0 \to \psi(2S)\pi^+ K^-$ and $\bar{B}^0 \to J/\psi\, \pi^+ K^-$ decays using a semi-model-independent approach (90, 93, 94). Without dependence on an amplitude model, this showed that these channels cannot be described only using conventional kaon excitations decaying to the $\pi^+ K^-$ final state. However, such an approach does not provide a complete picture of possible exotic contributions.

The LHCb data collected between 2011 and 2018, corresponding to an integrated luminosity of 9 fb^{-1}, yield 2.3 million and 140,000 reconstructed $\bar{B}^0 \to X\pi^+ K^-$ candidates, where X is respectively a J/ψ or $\psi(2S)$ state (72- and 6-fold increases, respectively). No amplitude analyses of the two decays together in the full LHCb dataset have yet been published, but unofficial results are available in the form of a PhD thesis (95). A large number (six to ten) of relatively broad, exotic $\psi(nS)\pi^+$ and $\psi(nS)K^-$ states of various J^P values is required for a good description of the data. Conceivably, such states can be explained by means of direct color couplings among the four quarks of a compact tetraquark system. In such states, the charm quark and antiquark share the

same confinement volume and can relatively easily fuse to form the $\psi(nS)$ state. This is in contrast to molecular charm meson–antimeson pairs, where decays to the $\psi(nS)$ state are suppressed. There is no clear evidence for production of the likely molecular narrow $Z_c(3900)^+$ and $Z_c(4020)^+$ states in $\bar{B}^0 \to \psi(nS)\pi^+K^-$ decays (18). Comparing the two amplitude analyses, except for the parameters of the $Z_c(4200)^+$ state, the masses, widths, and exact J^P composition of the resonances do not align well (95). This may be because coupled-channel effects, though expected, have not yet been accounted for in the amplitude fits. Direct three-body decays also have been neglected. Until more satisfactory amplitude models have been developed with better correspondence between the J/ψ and $\psi(2S)$ decays, discussion of the related exotic states should be approached with care. This applies especially to the 1^+ wave [including the $Z_c(4430)^+$ and $Z_c(4200)^+$ structures], which requires the largest number of poles to describe the LHCb data and, at the same time, is expected to couple to the $D\bar{D}^*$ and $D^*\bar{D}^*$ channels in an S-wave. Improvements to the amplitude models applied to the large LHCb $\bar{B}^0 \to \psi(nS)\pi^-K^+$ datasets are being pursued, and updated results are expected to be published in the future.

In 2009, the CDF experiment reported evidence of a very narrow ($\Gamma = 12 \pm 9$ MeV) near-threshold $X(4140)$ structure decaying to the $J/\psi\phi$ final state in 58 ± 10 reconstructed $B^- \to J/\psi\phi K^-$ decays. This report, using a dataset corresponding to an integrated luminosity of 2.7 fb^{-1} of $p\bar{p}$ Tevatron data (96), triggered a series of further investigations into the nature of resonances contributing to the decay (97–103). A charmonium state at this mass is expected to have a large decay width to an open-charm pair, and thus the narrow width and decay to the $J/\psi\phi$ state pointed to the exotic nature of the $X(4140)$ particle (96). The first result from LHCb data collected in 2010 (corresponding to an integrated pp luminosity of just 0.37 fb^{-1}) involved the study of 382 ± 22 reconstructed $B^- \to J/\psi\phi K^-$ decays and did not confirm the existence of the narrow $X(4140)$ state (99). The CMS Collaboration reconstructed $2{,}480 \pm 160$ of the decays in a dataset corresponding to an integrated luminosity of 5.2 fb^{-1} and observed the narrow (28 ± 24 MeV) $X(4140)$ state with high significance (101). Results from the CDF (98), CMS (101), and D0 (103) Collaborations also indicated a second, relatively narrow $J/\psi\phi$ state in the range of 4,274 to 4,328 MeV. All these results were obtained by performing simple fits to the $J/\psi\phi$ invariant mass distributions with significant assumptions about the background shapes in the signal regions. The first six-dimensional amplitude analysis of $B^- \to J/\psi\phi K^-$ decays, modeling the backgrounds as reflections of various kaon excitations, $K^{*-} \to \phi K^-$, was performed by the LHCb Collaboration using approximately 4,000 reconstructed decays. Only data collected during 2011 and 2012 data taking were included, corresponding to an integrated luminosity of 3 fb^{-1} (104, 105). Four prominent $J/\psi\phi$ resonances were needed for a good description of the data, including the $X(4140)$ threshold structure, albeit with significantly larger width (83 ± 30 MeV) than those obtained by the other experiments without amplitude analysis. Its quantum numbers were determined to be $J^{PC} = 1^{++}$. The second $J/\psi\phi$ structure, $X(4274)$, was confirmed and assigned the same quantum numbers. Two further new states, $X(4500)$ and $X(4700)$, were found with 0^{++} quantum numbers. The amplitude analysis was updated to the full 2011–2018 LHCb dataset in 2021, in which approximately 24,000 $B^- \to J/\psi\phi K^-$ decays were reconstructed with improved purity (106). The amplitude fit projections onto subsystem masses are shown in **Figure 5**. The four broad $J/\psi\phi$ mass peaks indicate the contributions from the $X(4140)$, $X(4274)$, $X(4500)$, and $X(4700)$ particles. A broad $J/\psi K^-$ mass peak at about 4 GeV suggests a contribution from an explicitly exotic $J/\psi K^-$ structure—a tetraquark candidate with minimal quark content ($c\bar{c}u\bar{s}$). From the amplitude analysis, this $J^P = 1^+$ $Z_{cs}(4000)^-$ state has a mass of $4{,}003 \pm 6^{+4}_{-14}$ MeV and a width of $131 \pm 15 \pm 26$ MeV. This is likely a different state than the narrow ($\Gamma \approx 8$–13 MeV) $Z_{cs}(3985)^{-,0}$ state observed by the BES III experiment in decays to $D_s^- D^{(*)}$ states. Properties of all the potentially exotic components in the LHCb amplitude model are summarized in **Table 2**. In addition to all four $X \to J/\psi\phi$ states observed

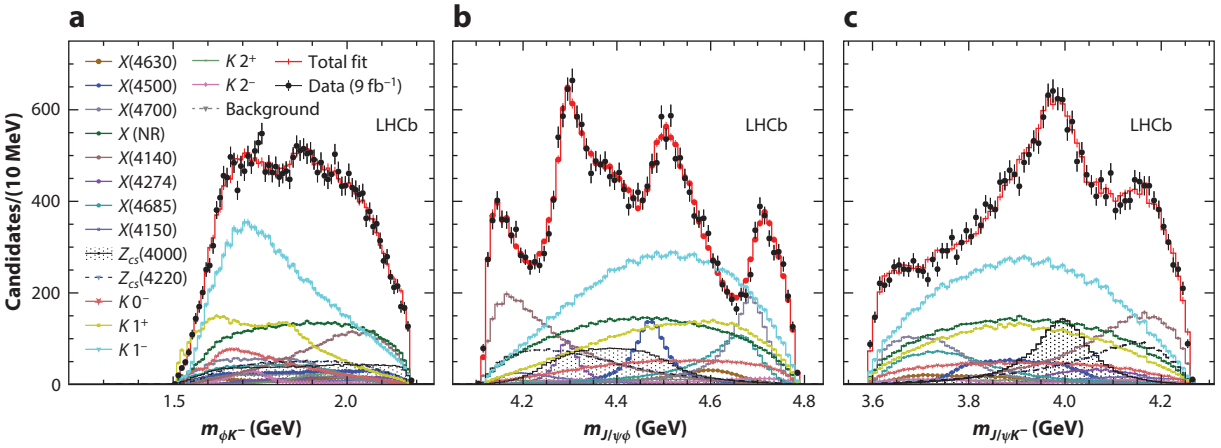

Figure 5

Distributions of the (*a*) ϕK^-, (*b*) $J/\psi\phi$, and (*c*) $J/\psi K^-$ invariant masses from the $B^- \to J/\psi\phi K^-$ data sample collected in the LHCb experiment during Runs 1 and 2 (106). Black dots with error bars show the data distribution. Projections of the amplitude fit are overlaid. Contributions from different intermediate structures are presented using different line colors, as indicated in the legend. Four peaks clearly visible in the $J/\psi\phi$ mass spectrum are described using the $X(4140)$, $X(4274)$, $X(4500)$, and $X(4700)$ states, which were previously observed using LHCb Run 1 data (104, 105). A broad peak at 4 GeV in the $J/\psi K^-$ mass spectrum corresponds to the $Z_{cs}(4000)^-$ tetraquark candidate. The amplitude model also includes the $X(4150)$, $X(4630)$, $X(4685)$, and $Z_{cs}(4220)^-$ exotic states and conventional kaon excitations, which are needed to reach a good description of the multidimensional data. Abbreviation: NR, nonresonant. Figure adapted from Reference 106 (CC BY 4.0).

using the 2011–2012 data (104, 105), there are several other exotic candidates that do not generate a visible peaking state in two-body final-state invariant mass spectra (**Figure 5**) but that are found to significantly improve the fit quality. They include the 2^{-+} $X(4150)$, 1^{++} $X(4685)$, and 1^{-+} $X(4630)$ states decaying to the $J/\psi\phi$ final state, and the 1^+ $Z_{cs}(4220)^-$ state decaying to the $J/\psi K^-$ final state.

After the observation of the $Z_{cs}(4000)^-$ tetraquark candidate (106), the LHCb Collaboration also performed an amplitude analysis of $B^0 \to J/\psi\phi K^0_S$ decays (107). Due to the lower reconstruction efficiency of K^0_S compared to that of K^- particles with the LHCb detector, the $B^0 \to J/\psi\phi K^0_S$ signal yield is one order of magnitude lower than the $B^- \to J/\psi\phi K^-$ signal yield, which makes it hard to perform a completely independent amplitude analysis of the B^0 decays. Assuming isospin symmetry, a simultaneous amplitude analysis was performed of both the $B^0 \to J/\psi\phi K^0_S$ and $B^- \to J/\psi\phi K^-$ decays, where most of the line-shape and coupling parameters were shared

Table 2 Properties of exotic hadrons contributing to the $B^- \to J/\psi\phi K^-$ decay (106)

J^P	Component	Significance	M_0 (MeV)	Γ_0 (MeV)	Fit fraction (%)
2^-	$X(4150)$	4.8σ	$4{,}146 \pm 18 \pm 33$	$135 \pm 28^{+59}_{-30}$	$2.0 \pm 0.5^{+0.8}_{-1.0}$
1^-	$X(4630)$	5.5σ	$4{,}626 \pm 16^{+18}_{-110}$	$174 \pm 27^{+134}_{-73}$	$2.6 \pm 0.5^{+2.9}_{-1.5}$
0^+	$X(4500)$	20σ	$4{,}474 \pm 3 \pm 3$	$77 \pm 6^{+10}_{-8}$	$5.6 \pm 0.7^{+2.4}_{-0.6}$
	$X(4700)$	17σ	$4{,}694 \pm 4^{+16}_{-3}$	$87 \pm 8^{+16}_{-6}$	$8.9 \pm 1.2^{+4.9}_{-1.4}$
1^+	$X(4140)$	13σ	$4{,}118 \pm 11^{+19}_{-36}$	$162 \pm 21^{+24}_{-49}$	$17 \pm 3^{+19}_{-6}$
	$X(4274)$	18σ	$4{,}294 \pm 4^{+3}_{-6}$	$53 \pm 5 \pm 5$	$2.8 \pm 0.5^{+0.8}_{-0.4}$
	$X(4685)$	15σ	$4{,}684 \pm 7^{+13}_{-16}$	$126 \pm 15^{+37}_{-41}$	$7.2 \pm 1.0^{+4.0}_{-2.0}$
1^+	$Z_{cs}(4000)^-$	15σ	$4{,}003 \pm 6^{+4}_{-14}$	$131 \pm 15 \pm 26$	$9.4 \pm 2.1 \pm 3.4$
	$Z_{cs}(4220)^-$	5.9σ	$4{,}216 \pm 24^{+43}_{-30}$	$233 \pm 52^{+97}_{-73}$	$10 \pm 4^{+10}_{-7}$

between these two channels, except for those related to the $Z_{cs}(4000)^-$ and $Z_{cs}(4000)^0$ states. Evidence at the level of 4σ was seen for a $Z_{cs}(4000)^0$ state, which had a mass and width consistent with those of the $Z_{cs}(4000)^-$ particle (107).

A simple fit to the high-mass peaking structure led the LHCb Collaboration to conclude the presence of a $J/\psi\phi$ state with a mass of 4,741 ± 6 ± 6 MeV and a width of 53 ± 15 ± 11 MeV in a study of $B_s^0 \to J/\psi\phi\pi^+\pi^-$ decays (28).

While $Z_{cs}^- \to J/\psi K^-$ states are minimally four-quark objects, the $X \to J/\psi\phi$ states could be conventional $c\bar{c}$ states, $c\bar{c}s\bar{s}$ tetraquarks, or $c\bar{c}g$ hybrids. The $X(4140)$ state, which was initially claimed to have a very narrow width (96, 98), has a width of $162 \pm 21^{+24}_{-49}$ MeV as determined by the latest LHCb analysis. Nevertheless, its high fit fraction in the phase-space-suppressed region makes it a probable $c\bar{c}s\bar{s}$ candidate. The quantum number pattern of the observed $J/\psi\phi$ states does not fit the expectations for charmonia, making it likely that the compact tetraquark dynamics is involved, possibly mixing in with high radial excitations of the $c\bar{c}$ states. As with the $\bar{B}^0 \to \psi(nS)\pi^+K^-$ decays discussed above, the amplitude analysis of $B^- \to J/\psi\phi K^-$ performed by the LHCb experiment did not include coupled-channel terms from $D_s^{(*)}\bar{D}_{(s)}^{(*)}$ pairs, nor did it include three-body contributions; thus, the exact spectral decomposition of the obvious $J/\psi\phi$ and $J/\psi K^-$ mass structures may contain model-dependent biases.

Recently, the LHCb Collaboration has detected $B^- \to D_s^+ D_s^- K^-$ decays for the first time (reconstructing roughly 360 candidates) and performed an amplitude analysis (108). A significant (much more than 5σ) near-threshold peak is seen in the $D_s^+ D_s^-$ mass spectrum, which can be modeled as a 0^{++} $X(3960)$ state at 3,956 ± 5 ± 10 MeV with a rather narrow width of 43 ± 13 ± 8 MeV (109). There is also a possible 0^{++} state at 4,133 ± 6 ± 6 MeV with a relatively narrow width ($\Gamma = 67 \pm 17 \pm 7$ MeV), generating the $D_s^+ D_s^-$ invariant mass dip via interference with a sizeable nonresonant component. An alternative way to describe the mass dip is to use the K-matrix line shape for the $X(3960)$ state, including the coupling to the $J/\psi\phi$ channel. The $X(3960)$ state is too narrow to be a 3^3P_0 charmonium state.

6. CHARMING AND STRANGE TETRAQUARK CANDIDATES

Conventional states that involve a charm quark and a strange antiquark are well established, but no evidence for corresponding states that include a charm quark and a strange quark had arisen before 2020. Bound states containing both a charm and a strange quark would be manifestly exotic, requiring at a minimum four quarks to form a color-singlet state. Experimental context aside, few suggestions had been made for their existence even in the theoretical literature before that point (110–112).

Experimental evidence for bound states that contain both a charm quark and a strange quark first emerged in studies published by the LHCb Collaboration (113, 114) involving $B^\pm \to D^+D^-K^\pm$ decays with the charm mesons reconstructed in their decays to the $K^-\pi^+\pi^+$ final state. Care was taken to ensure that the combinatorial backgrounds that often plague high-multiplicity, fully hadronic final states (the feed-down from three-kaon or four-pion charm meson decays) were heavily suppressed. The LHCb PID system was effective at reducing backgrounds from pion–kaon misidentification, and the particular topology of the decay—two long-lived charged D mesons—allowed effectively all background from charmless and single-charm decays to be removed. Two methods were used to analyze the three-body phase space of the $B^\pm$ decay.

The first approach (113) built on the expectation that conventional resonances would appear only in the D^+D^- channel, not in the D^+K^- ($cs\bar{u}\bar{d}$) or doubly charged D^+K^+ ($c\bar{s}u\bar{d}$) channels—a semi-model-independent treatment, similar to that previously used in the analysis of other three-body b hadron decays featuring only one two-body decay chain in which conventional

resonances were expected (48, 89, 90, 93). The approach involved assessing how well the data in the entire phase space could be described assuming the presence of resonances in the D^+D^- channel. The phase space was divided into slices of D^+D^- invariant mass, and the helicity angle was decomposed in terms of the orthogonal basis of Legendre polynomials. The spin component of the amplitude for contributing resonances would be expected to give rise to a helicity structure that could be described using a finite set of Legendre polynomials, the size of which would correspond to the maximum spin of the D^+D^- resonances in that slice. A limit on the order of the Legendre polynomials available for the decomposition was introduced, motivated by the fact that very-high-spin (>3) intermediate states are unlikely to be formed during the decay of a pseudoscalar particle to three more pseudoscalars. A recombination of the descriptions obtained in each slice allows a test of how well the phase space has been described as well as the possibility to test the success of that description in different projections of the phase space. Poor agreement was observed; the disagreement was most marked when the D^+K^- projection of the phase space was considered, particularly in the region of invariant mass near 2.9 GeV.

To characterize the exotic hadron contributions, the second approach involved a full amplitude analysis of the three-body phase space (114). An amplitude was constructed that consisted of known charmonium resonances (modeled by a relativistic Breit–Wigner function in invariant mass with a helicity structure corresponding to the resonance spin) and a nonresonant component. Complex coefficients multiplying each resonance were free to vary, but only a rather poor description of the data was achieved. Only when two new amplitudes were added in the D^+K^- spectrum, with quantum numbers $J^P = 0^+$ and 1^-, was an adequate description obtained (see **Figure 6**). The two new amplitudes corresponded to $T_{cs0}(2900)^0$ and $T_{cs1}(2900)^0$ resonant components with masses of 2,866 ± 7 ± 2 and 2,904 ± 5 ± 1 MeV and widths of 57 ± 12 ± 4 and 110 ± 11 ± 4 MeV for the 0^+ and 1^- states, respectively.

The interpretation of the two new amplitudes in the D^+K^- channel has not been easy. Much speculation has focused on the proximity of the new states to the $\bar{D}^*K^*$ and $\bar{D}_1K$ thresholds: 2,902 and 2,913 MeV, respectively (115). Compact tetraquark explanations often yield states with expected masses well below the slightly lighter observed 0^+ state (116). Difficulty has been

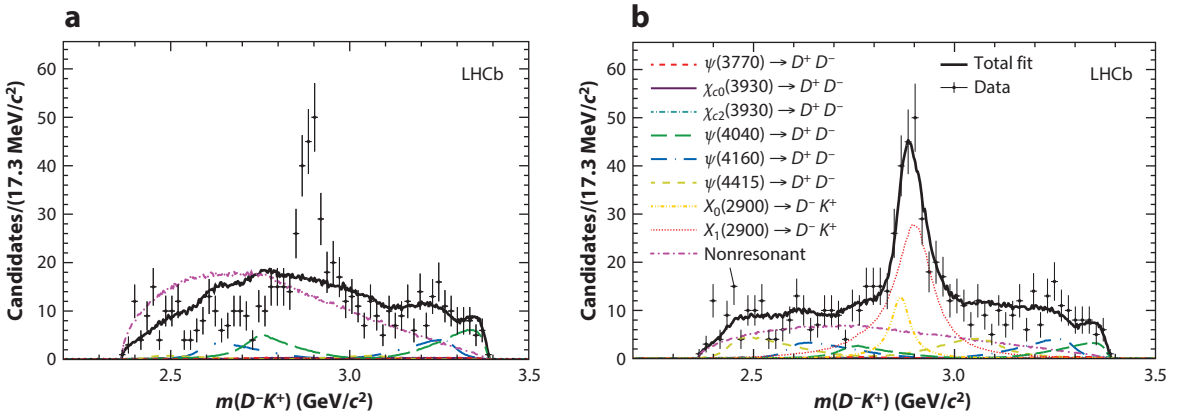

Figure 6

Invariant mass distributions of D^-K^+ pairs in the decay $B^+ \to D^+D^-K^+$ (*black points*). (*a*) The data are fitted with an amplitude model (*solid black line*) that consists of resonances only in the D^+D^- channel. Individual model components are indicated by colored lines. A severe discrepancy is observed around 2.9 GeV. (*b*) Resonant components are added to the model in the D^-K^+ channel, and an adequate description is achieved. Figure adapted from Reference 114 (CC BY 4.0).

encountered in accounting for both the 0^+ and 1^- states within a single $\overline{D}^* K^*$ or $\overline{D}_1 K$ molecular picture, although more progress has been made when these have been treated separately (117). Attempts have also been made to accommodate the structures as the products of coupled-channel kinematic effects that arise from rescattering processes (118).

To make progress in understanding the unexpected structures, a close partnership between experiment and theory may prove fruitful. The first study by the LHCb Collaboration employed data taken between 2011 and 2018, but an increase of at least an order of magnitude in the size of the dataset available to pursue these particular B^+ decays can be anticipated during Runs 3 and 4. Furthermore, the LHCb Collaboration will not be alone in acquiring datasets of interest to engage these processes: The Belle II Collaboration is well placed to make important contributions here, too, with their higher absolute track reconstruction efficiency making up in high-multiplicity final states for much lower $B^\pm$ production rates. A significant opportunity exists for experimentalists and theorists to implement new theoretical models early on in the analysis of ever-growing data samples.

The study of other decays is also highly likely to shed light on the nature of the $T_{cs}(2900)^0$ structures. In particular, the results of a future study of $B^+ \to D^+ K^- \pi^+$ decays (113, 114) and a future first revealing of the LHCb data for $B^0 \to D^+ \overline{D}^0 K^-$ decays are obvious candidates, both sharing the channel of interest in the discovery study.

Although at face value the study of decays involving a $D_s^+ \pi^-$ channel ($c\bar{s}u\bar{d}$) seems only indirectly connected to that of $B^+ \to D^+ D^- K^+$ decays, a remarkable parallel has emerged that led to the discovery of the $T_{c\bar{s}0}(2900)$ states. The LHCb Collaboration undertook amplitude analyses of the decays $B^0 \to \overline{D}^0 D_s^+ \pi^-$ and $B^+ \to D^- D_s^+ \pi^+$—processes in which conventional $q\bar{q}$ resonances would be expected only in the $\overline{D}^0 \pi^-$ or $D^- \pi^+$ channels (119, 120). The two datasets were fitted simultaneously, where isospin relationships were imposed between corresponding amplitudes in the two channels. The Dalitz plot visualization of the decay phase space clearly illustrates the similarity of the resonant structure. Resonant amplitudes, modeled again by relativistic Breit–Wigner functions, were introduced that corresponded to various excited open-charm states, and a quasi-model-independent spline function was used to model the nonresonant S-wave contribution. The model fails to describe the phase space well, particularly in the region around a mass of 2.9 GeV in the $D_s^+ \pi^-$ and $D_s^- \pi^+$ spectra in the $B^0 \to \overline{D}^0 D_s^+ \pi^-$ and $B^+ \to D^- D_s^+ \pi^+$ decays, respectively. A good fit quality is achieved through the addition of two new $D_s^+ \pi^-$ states, sharing a complex coefficient, mass, and width, according to isospin symmetry expectations. The best fit was achieved with a spin-parity of $J^P = 0^+$, and the fitted mass and width of the new states, named $T^a_{c\bar{s}0}(2900)^0$ and $T^a_{c\bar{s}0}(2900)^{++}$, are 2,909 ± 10 and 134 ± 19 MeV, respectively. An encouraging confirmation of the resonant character of the new state was obtained through the use of a spline function to model the S-wave component in the $D_s^- \pi^+$ channel. Plotting the amplitude at the knots of the spline function (**Figure 7**), it is observed that the amplitude follows a trajectory consistent with that expected for a resonance in the channel as a function of the $D_s^- \pi^+$ invariant mass.

It is interesting that the earlier study of the $D^+ K^+$ channel in the $B^+ \to D^+ D^- K^+$ decay did not motivate the introduction of a doubly charged contribution, though the sample size was considerably smaller in that case (113, 114). In fact, an excess was observed at a mass of 2.9 GeV in the $D^+ K^+$ channel in that analysis, but it was adequately described as the reflection of the spin-2 $\chi_{c2}(3930)$ component of the amplitude model. It will be of interest whether the description remains satisfactory as the larger Run 3 dataset is brought into view. As for the states discovered in the $D^+ D^- K^+$ final state, the use of single-charm decays is likely to be of considerable value here—in this case, $B^- \to D_s^+ K^- \pi^-$, where the $D_s^+ \pi^-$ channel appears once more.

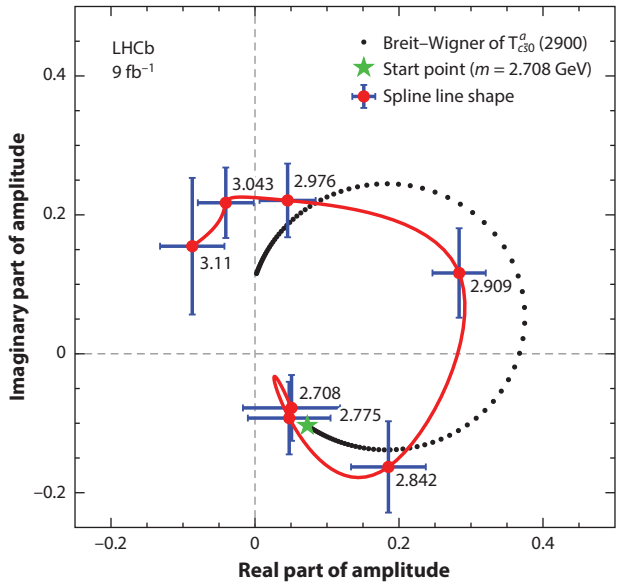

Figure 7

Argand diagram showing the complex coefficients associated with a spline function used to describe the S-wave component in the $D_s^- \pi^+$ channel. The amplitude follows a trajectory consistent with that expected for a resonant contribution in that S-wave channel (approximately circular counterclockwise mass evolution). Figure adapted from Reference 119 (CC BY 4.0).

The claim for observation of a new isospin pair of states, with one electrically neutral and one doubly charged, was a striking one. The relationship between the above-discussed $T_{cs}(2900)^0$ structures and the new $T^a_{c\bar{s}0}(2900)$ states is not obvious; aside from the differing quark content, their widths also differ significantly. Interpretation of the new states followed a pattern similar to that of the $T_{cs}(2900)^0$ states, with models ranging from compact tetraquarks to molecular models (121, 122), once more noting the proximity of the 2.9-GeV structure to the D^*K^* threshold and to that of the $D_s^*\rho$ combination (117). Attempts have also been made to provide a unified description of the D^+K^- and $D_s^+\pi$ states as part of a new $SU(3)$ flavor sextuplet, though the absence of a corresponding nonstrange $D^*(2900)^0$ state is notable (123).

7. HIDDEN-DOUBLE-CHARM TETRAQUARK CANDIDATES

If the discoveries outlined in Section 6 had been made earlier, those tempted to apply a molecular interpretation to the excesses observed near meson-pair thresholds might have been less surprised by evidence of a new structure near the threshold in the invariant mass spectrum of promptly produced pairs of J/ψ mesons (124). It was, however, the searches for tetraquark states comprising four heavy beauty quarks ($bb\bar{b}\bar{b}$) decaying to $(\Upsilon(1S) \to \mu^+\mu^-)\mu^+\mu^-$ states (125, 126) that had captured the attention of experimentalists before the LHCb Collaboration turned to look for $cc\bar{c}\bar{c}$ states. Such states might be expected to decay into a pair of J/ψ (or other charmonium) mesons, each composed of a $c\bar{c}$ pair. Predictions for such states were already in place in the range from 5.8 to 7.4 GeV (127–143).

A search for tetraquark states decaying to the $(J/\psi \to \mu^+\mu^-)(J/\psi \to \mu^+\mu^-)$ final state was undertaken by the LHCb Collaboration using the full LHCb 2011–2018 dataset (9 fb^{-1}). The sample preparation was relatively straightforward; it consisted of momentum thresholds for momentum

tracks, standard muon identification, and the requirement that pairs of oppositely charged muon tracks form a reasonable vertex with an invariant mass from 3 to 3.2 GeV. A further requirement that the J/ψ candidates be consistent with an origin at the primary pp collision point suppressed the background from B decays, thanks to the displaced production point for candidates produced via those processes. The possibility for muon tracks to be used twice in reconstructing the $J/\psi J/\psi$ pair was excluded simply by requiring a significant angular separation for the tracks.

The resulting sample contained a large fraction of correlated J/ψ candidates. Finally, the invariant mass spectrum of the J/ψ pair could be considered with improved resolution thanks to a kinematic refit with mass constraints on each J/ψ candidate. Because resonant J/ψ pair production is associated with single-parton scattering (SPS) as opposed to the independent J/ψ production of double-parton scattering (DPS), and because such SPS interactions are characterized by a higher transverse momentum for the J/ψ pair, it was easy to suppress the DPS background. The residual DPS production component was identified by exploiting the fact that it typically inhabits the high J/ψ-pair invariant mass region. The di-J/ψ spectrum displayed two peculiar features: a broad near-threshold structure and a second, narrower structure around 6.9 GeV [often referred to as $X(6900)$]. Both appeared to grow in significance as the transverse momentum of the J/ψ pair increased, and neither appeared to originate in efficiency structures, which were found to be rather flat as a function of invariant mass.

The interpretation of the structures is complicated and affects the functions applied in a fit to the di-J/ψ spectrum. Two models achieved a satisfactory description of the data. The first, shown in **Figure 8**, consisted of a single Breit–Wigner function corresponding to the higher-mass, narrower structure, and two more Breit–Wigner functions to describe the near-threshold shape. A second model allowed for interference between the component describing the nonresonant SPS production and the near-threshold resonance. The first model yields a measurement for the higher-mass state of 6,905 ± 11 MeV and a width of 80 ± 19 MeV, whereas the second produced a slightly lower mass of 6,886 ± 11 MeV and a width of 168 ± 33 MeV.

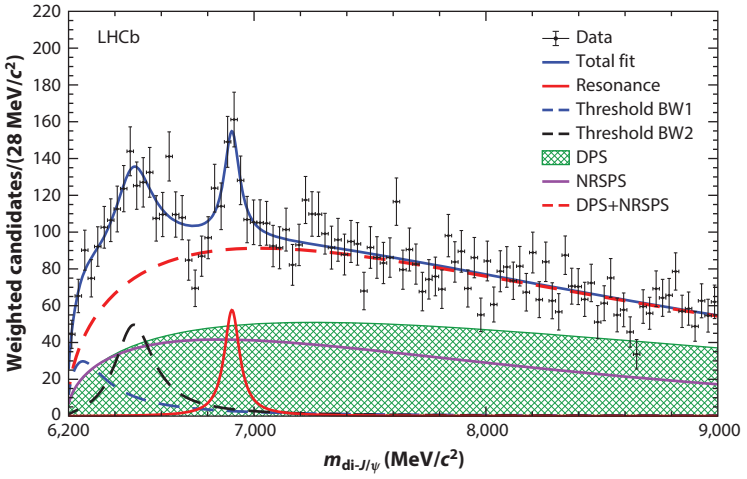

Figure 8

Fit to the $J/\psi J/\psi$ invariant mass spectrum according to the first of two models, where a single relativistic Breit–Wigner function is used to describe the higher-mass excess, and two more Breit–Wigner functions are used to describe the near-threshold region. Abbreviations: BW, Breit–Wigner; DPS, double-parton scattering; NRSPS, nonresonant single-parton scattering. Figure adapted from Reference 124 (CC BY 4.0).

Since no hadron identification is needed, and all LHC detectors are equipped with muon detectors, the $J/\psi J/\psi$ final state is also accessible to the ATLAS and CMS experiments (144, 145). The lower absolute reconstruction efficiencies, due to the higher muon transverse momentum thresholds, are offset by the higher integrated luminosities (135–140 fb^{-1}, Run 2) obtained by these central detectors collecting their data at the maximal LHC instantaneous luminosity. The LHCb discovery prompted these collaborations to analyze their $\mu^+\mu^-\mu^+\mu^-$ samples near the double-charmonium threshold with a superior sensitivity. The 6.9-GeV structure was confirmed by both experiments. In addition to the $J/\psi J/\psi$ structure, the ATLAS Collaboration has 4.7σ evidence for a $J/\psi\,\psi(2S)$ mass structure in a similar mass range (144). The CMS Collaboration found clear evidence for the lower-mass state at 6.6 GeV and 4.1σ evidence for a peak at 7.3 GeV (145).

Once more, the nature of the observed four-quark mass structure is unclear. Decomposition of the observed mass spectrum into resonant contributions is assumption dependent, though it is likely that multiple resonances play a role. Their widths are of the order of 100 MeV or more, unlike the tetraquark and pentaquark candidates—good candidates for the molecular states—discussed above. Both of these observations point to compact tetraquark dynamics. However, coupled-channel effects [e.g., from $J/\psi\,\psi(2S)$] can also play a role (146). The addition of the new, larger Run 3 dataset should shed light on some of these questions.

8. NARROW DOUBLE-CHARM TETRAQUARK

In 2017, the LHCb Collaboration observed a Ξ_{cc}^{++} state in its decay to the $\Lambda_c^+K^-\pi^+\pi^+$ final state with a mass of approximately 3,621 MeV (147). The signal consisted of 313 $\pm$ 33 candidates and had overwhelming significance in Run 2 data corresponding to an integrated luminosity of 1.7 fb^{-1}. Later analysis of the full Run 2 dataset—approximately three times larger—confirmed observation of the state in the $\Lambda_c^+K^-\pi^+\pi^+$ and $\Xi_c^+\pi^+$ decay modes with a combined yield exceeding 2,000 candidates (148). Together with the observation of hundreds of signal candidates for the $X(6900)$ state decaying to $J/\psi J/\psi$ states (see Section 7), this indicated that the LHCb data sample could be used to search for even more rare hadronic states containing two charm quarks, including tetraquark states formed by two charm quarks and two light antiquarks. These states have been awaited since the 1980s (129, 149) as candidates for a tightly bound exotic hadron state. The measured mass of the Ξ_{cc}^{++} baryon enabled the refinement of models of binding of doubly heavy diquarks and implied that the mass of the $cc\bar{u}\bar{d}$ tetraquark should be close to the sum of the D and D^* masses (150) and therefore might be narrow, providing a clear experimental signature. Also, in analogy to the number of narrow tetraquark states seen in $D^{(*)}\bar{D}^{(*)}$ spectra near the corresponding mass thresholds [e.g., $\chi_{c1}(3872)$, $Z_c(3900)$], one might expect similar molecular states near the $D^{(*)}D^{(*)}$ thresholds. At the same time, no consensus regarding these states existed, and theoretical predictions for the isospin-zero ground state ($cc\bar{u}\bar{d}$) varied within the range of $\pm$250 MeV around the D^0D^{*+} mass threshold.

Using the full Run 1 and 2 LHCb data sample, the mass spectra of various $DD(\pi^+)$ combinations, where D represents D^0 or D^+ produced directly in pp collisions, were analyzed (151, 152). Peaking structures were observed in the D^0D^0, D^0D^+, and $D^0D^0\pi^+$ mass spectra near the corresponding mass thresholds. The peak in the $D^0D^0\pi^+$ distribution appeared to lie a fraction of 1 MeV below the D^0D^{*+} threshold. It was narrower than the peak in the D^0D^+ channel and, as such, was the most natural candidate for the predicted ground ($cc\bar{u}\bar{d}$) tetraquark state, T_{cc}^+. Given the close proximity to the threshold, a simple Breit–Wigner function could not be used for the description of its shape. Instead, a unitarized Breit–Wigner model was constructed, taking into account coupled-channel effects and relying on two assumptions. The first assumption was that the observed state should decay strongly in the D^0D^{*+} and D^+D^{*0} channels and, subsequently,

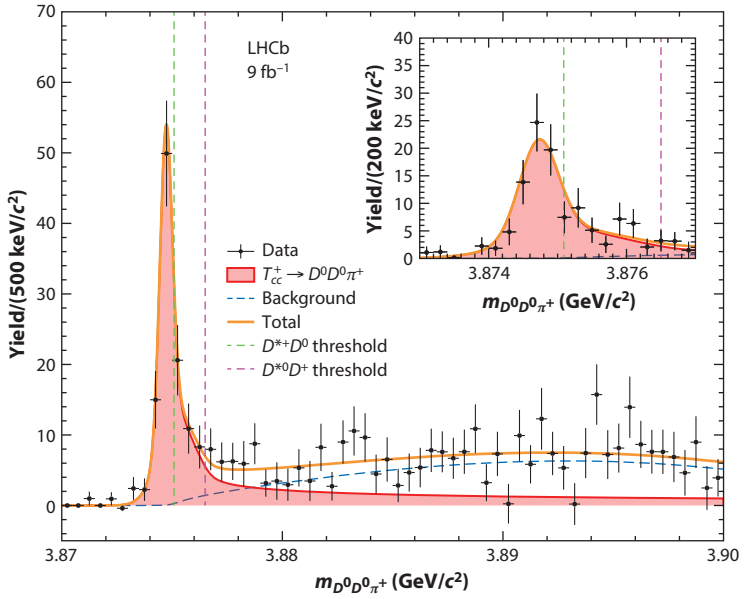

Figure 9

Fit to $D^0D^0\pi^+$ invariant mass with the T_{cc}^+ signal described as a unitarized Breit–Wigner function on top of a nonresonant background modeled by a phase-space term multiplied by a polynomial, all convolved with detector resolution. Figure adapted from Reference 151 (CC BY 4.0).

to $D^0D^0\pi^+$, $D^0D^+\pi^0$, and $D^0D^+\gamma$ final states, with equal couplings. Second, it was assumed to have isospin $I = 0$ and quantum numbers $J^P = 1^+$, in accordance with the theoretical expectation for the T_{cc}^+ ground state. In the derivation of the subsequent T_{cc}^+ line shape, unitarity is ensured by accounting for the energy dependence of the $D^0D^0\pi^+$, $D^0D^+\gamma$, and $D^0D^+\pi^0$ decay widths. Analyticity is ensured by accounting for the imaginary part of the total width via the Kramers–Kronig relations. The resulting function for the T_{cc}^+ line shape happens to depend on only one parameter—the mass position of the peak—given that the decay coupling to DD^* is large enough. The function is then convolved with a detector resolution of approximately 400 keV, which is an order of magnitude larger than the natural T_{cc}^+ width calculated in this model. The nonresonant D^0D^{*+} background in the fit to the data is assigned a phase-space model. The resulting model provides a good description of the data (see **Figure 9**). The mass of the state relative to the D^0D^{*+} threshold was measured to be $\delta m_{T_{cc}^+} = -359 \pm 40^{+9}_{-6}$keV. For this value of the mass, the model calculation gives a width of $\Gamma = 48 \pm 2^{+0}_{-14}$keV, where the first width uncertainty is due to that on the mass measurement, and the second is due to the uncertainty in the coupling parameter of the T_{cc}^+ to DD^*, $|g|$. While the lower limit reflects the experimental constraints, the upper one does not and is entirely a feature of the model—namely, that the width of the T_{cc}^+ saturates at high values of the coupling $|g|$.

Using the same T_{cc}^+ decay model with the T_{cc}^+ mass value determined from the fit to the $D^0D^0\pi^+$ channel, the expected T_{cc}^+ signal shapes in the D^0D^0, D^0D^+, and $D^0\pi^+$ mass distributions from T_{cc}^+ decays to the $D^0D^0\pi^+$, $D^0D^+\pi^0$, and $D^0D^+\gamma$ final states were obtained. In all cases, a good agreement with the data distributions was observed when fitting their amplitudes on top of the nonresonant backgrounds. Together with nonobservation of any peaking structures in the D^+D^+ and $D^+D^0\pi^+$ mass spectra, this provides additional support for the assumed T_{cc}^+ decay model and, in particular, for the assumption that the discovered state is an isoscalar. In

addition, the dependence of T_{cc}^+ production on its transverse momentum and event track multiplicity was studied. It was compared to the production of D^0D^0 pairs with masses in the range of $3.75 < m_{D^0D^0} < 3.87$GeV, expected to have a large contribution from DPS, and of $D^0\overline{D}^0$ pairs with masses below 3.87 GeV, given the similarity to charmonium production. While $\chi_{c1}(3872)$ production was found to be suppressed with respect to $\psi(2S)$ production at high multiplicities (see **Figure 3**) (34), no such suppression was observed for the T_{cc}^+ state. This suggests that different mechanisms might play roles in their production. However, given the low statistics, no firm conclusions could be made.

The T_{cc}^+ state is very close to the D^0D^{*+} threshold (see **Figure 9**), a fact that is reminiscent of the $\chi_{c1}(3872)$ state being close to the $D^0\overline{D}^{*0}$ threshold. As for the $\chi_{c1}(3872)$ state, it is natural to assume that the T_{cc}^+ state is predominantly a loosely bound DD^* molecule, which matches the theoretical predictions based on the nonrelativistic constituent quark model made a long time before the T_{cc}^+ discovery (153). However, since compact tetraquark models predict that the T_{cc}^+ mass also would be in this range, both configurations might play a role. At the same time, a good description of the $D^0D^0\pi^+$ mass spectra by the model assuming only $T_{cc}^+ \to DD^*$ decays (discussed above) does not leave much room for nonresonant $T_{cc}^+ \to DD\pi(\gamma)$ decay modes, which are expected to be sizeable for a compact tetraquark. Compared to the T_{cc}^+ state, the $\chi_{c1}(3872)$ state has an order-of-magnitude-larger width, it decays to the lighter charmonium states, and it can contain an admixture of the conventional charmonium state itself. This makes the T_{cc}^+ state much simpler for theoretical description and allows for less ambiguous interpretation of its experimentally measured properties. Hence, it has great potential for helping to identify the relative roles of compact tetraquark and molecular configurations.

9. FUTURE PROSPECTS

During Runs 1 and 2, the LHCb experiment successfully operated at instantaneous luminosities reaching $\mathcal{L} \approx 4 \times 10^{32}\,\mathrm{cm}^{-2}\,\mathrm{s}^{-1}$ and produced excellent results. To cope with higher instantaneous luminosity while maintaining or improving detection efficiency, a major upgrade of the detector has been installed during Long Shutdown 2 (154). The new detector is now in place.

Increased luminosity will result in signal rates that exceed 1 MHz, which previously was the maximum output rate of the hardware (level 0) trigger of the original detector. If a similar hardware trigger had been used, it would have resulted in a large loss of the signal efficiency, devaluing the gain from the higher luminosity, especially for fully hadronic channels. To overcome this limitation, the level 0 trigger was eliminated, thus for the first time introducing a full software trigger and readout of the entire detector at the visible LHC beam–beam collision rate of 30 MHz. This enables discrimination of signals from the backgrounds based on full event reconstruction. Hence, trigger efficiencies are kept as high as in Runs 1 and 2 or, in cases of fully hadronic channels, are even doubled. This new approach required migrating the first stage of the partial event reconstruction to a farm of GPU-equipped compute nodes and speeding up the rest of the event reconstruction via efficient use of memory allocations and multithreading. To cope with the increased number of beam–beam interactions per beam crossing, and thus detector occupancy, the experiment's tracking system was completely upgraded. A new vertex detector is made of an array of silicon pixel detectors, which replace the silicon strips used before the upgrade. The inner radius was decreased from 8.2 to 5.1 mm. The silicon-strip tracker in front of the dipole magnet has a much improved readout segmentation and also extends closer to the beam pipe. The tracker behind the magnet, which used to be a combination of silicon strips in the inner part and straw tubes in the outer part, was replaced by scintillating fibers. All sensors, including new photodetectors in the RICH detectors (multianode PMTs instead of

HPDs), are now read out at the 40-MHz beam-crossing frequency. The new nominal luminosity should reach $\mathcal{L} \approx 2 \times 10^{33}\ \mathrm{cm}^{-2}\ \mathrm{s}^{-1}$, and a total integrated luminosity of approximately 50 fb^{-1} is expected by the end of Run 4 of the LHC (including Runs 1 and 2). Together with improved trigger efficiency, the total yields in most physics channels will be an order of magnitude larger than in Runs 1 and 2. This opens vast opportunities for the extension of exotic hadron studies.

For various b decays to final states that contain a J/ψ or $\psi(2S)$ meson decaying to a $\mu^+\mu^-$ state, signal yields will reach millions of events. For final states with other types of charmonium states decaying to hadrons, like η_c or $\chi_{c0,1,2}$ decaying to $p\bar{p}$ states, which have relatively low branching fractions and lower trigger efficiencies, signal yields will reach up to hundreds of thousands of events. This will allow for precise characterization of already-discovered tetraquark and pentaquark states with hidden charmonium. At the same time, signal yields for b decays to final states with double open charm (e.g., $D\bar{D}$, $\Lambda_c^+\bar{D}$) will reach tens of thousands of events and allow for the observation of tetraquarks and pentaquarks in these modes. That will open the way to constrain coupled-channel effects in their various decay modes and, eventually, a joint description of corresponding decay amplitudes via, for instance, the K-matrix formalism.

In relation to exploration of the $\chi_{c1}(3872)$ state, the larger dataset would allow precise determination of relative branching fractions of its various decays and access to new suppressed decay modes (e.g., $\chi_{c1}\pi^+\pi^-$, $p\bar{p}$). Moreover, decays of other exotic states to the $\chi_{c1}(3872)$ state may be discovered. Improved studies of the $\chi_{c1}(3872)$ mass line shape in selected decay channels will elucidate the nature of the $\chi_{c1}(3872)$ state. With the SMOG system (155) capable of injecting various noble gases into the volume of the LHCb vertex detector, studies of $\chi_{c1}(3872)$ production can be extended to a larger number of colliding systems.

Runs 3 and 4 will also make possible the detailed study of doubly charmed exotic states—namely, T_{cc}^+ and resonances in the $J/\psi J/\psi$ system—and searches for analogous states with beauty quarks. They will also increase prospects for studies of exotic states with hidden beauty, so far observed only in e^+e^- collisions, and searches for other types of exotic states like tetra/pentaquarks decaying only weakly or hadrons formed by six quarks.

To exploit the High-Luminosity LHC (HL-LHC), a further upgrade (Upgrade II) is planned for Long Shutdown 4 (156). After the second upgrade, the detector will operate at a maximum instantaneous luminosity of $\mathcal{L} \approx 1.5 \times 10^{34}\ \mathrm{cm}^{-2}\ \mathrm{s}^{-1}$ with a plan to integrate a dataset corresponding to an integrated luminosity of 300 fb^{-1} by the end of data collection, thus increasing statistics in most channels by another order of magnitude. The LHCb experiment will be capable of studying exotic hadrons with charm in decays of any b hadron up to the B_c^+ meson and in almost all conceivable final states, which otherwise will not be accessible in any other experiment foreseen in the coming decades. For a number of exotic states, double-differential measurements of their production cross sections will be performed, together with measurements of their dependence on the collision environment. Potentially, the obtained experimental knowledge will reach a volume and quality to allow a profound understanding of the nature of the multiquark states and will help to improve knowledge of nonperturbative QCD.

While exotic hadron spectroscopy has a bright future in the LHCb program, other experimental programs have an important role to play in investigating exotic hadrons that may not be reachable at the LHC, such as the $\psi(4230)$ and $Z_b^{+,0}$ states (157).

10. CONCLUSION

The first generation of the LHCb experiment, which collected data over the past decade (Runs 1 and 2 at the LHC), had a profound impact on exotic hadron spectroscopy. This was achieved thanks to its unique capabilities (Section 2) to efficiently trigger on, and suppress backgrounds

in, final states containing heavy charm and beauty quarks at the LHC. The resulting heavy-quark dataset will be unrivaled for decades to come. The LHCb experiment demonstrated that many previously known exotic hadron candidates can be best studied at such a high-energy hadron collider despite the experimental complications stemming from the large number of particles produced in such an environment. The LHCb Collaboration's achievements in studies of the $\chi_{c1}(3872)$ particle (Section 3) are excellent examples, including definitely determining its quantum numbers; reaching the sensitivity to observe its natural line shape for the first time; providing precise clarification of the isopin-violating nature of its discovery mode, $\chi_{c1}(3872) \to \pi^+\pi^- J/\psi$; and uncovering evidence for the unusual particle-multiplicity dependence of its prompt production.

The improved sensitivity helped to demonstrate that many hidden-charm exotic hadrons previously observed in B meson decays, such as $Z_c(4430)^+ \to \psi(2S)\pi^+$ and $X(4140) \to J/\psi\phi$, were only the tip of the iceberg of a rich spectrum of similar states with various quantum numbers (Section 5). Exotic $J/\psi K^+$ resonances in the same B meson decays have been observed for the first time. None of these states are very narrow, qualitatively fitting the expectations of a compact tetraquark model, $c\bar{c}q\bar{q}$, in which there is no effective mechanism to prevent the charm quark and charm antiquark from finding each other to form a $\psi(2S)$ or J/ψ meson. Coupled-channel effects still need to be taken into account in the amplitude analyses used to extract their spectra before the spectral decomposition of these resonances is to be fully trusted. So far, there is no evidence for comparatively narrow molecular tetraquark states like the $Z_c(3900)^{+,0} \to J/\psi\pi^{+,0}$, so well established in e^+e^- production.

In contrast, among the most striking discoveries by the LHCb experiment are the relatively narrow pentaquark states $P_c^+ \to J/\psi p$ and $P_{cs}^0 \to J/\psi\Lambda$, matching the expectations for molecular states near the charm baryon + charm meson mass thresholds (Section 4). Whether broader pentaquark states matching compact pentaquark spectroscopy exist is an open experimental question. These hidden-charm pentaquarks have been observed in b baryon decays, which are not reachable at the e^+e^- B factories.

Less clear is the origin of the charmed and strange tetraquark candidates discovered by the LHCb experiment in B meson decays (Section 6). The Belle II experiment has good prospects to contribute here.

The other frontier opened by the LHCb experiment concerns $cc\bar{c}\bar{c}$ states observed in prompt productions and decaying to vector charmonium pairs (Section 7). Since the latter are detected in the $(\mu^+\mu^-)(\mu^+\mu^-)$ final state, the ATLAS and CMS experiments have a good sensitivity to them. Both experiments confirmed the mass structures discovered by the LHCb Collaboration and contributed additional evidence for the states. These structures are not unlikely to be due to compact tetraquark dynamics, though coupled-channel effects may also play a role.

Last but not least, the LHCb experiment also discovered the narrowest exotic hadron known to date, the $T_{cc}^+ \to D^0D^0\pi^+$ (Section 8), carrying two units of charm ($cc\bar{u}\bar{d}$). Having some similarities with the $\chi_{c1}(3872)$ state, due to the proximity to the DD^* threshold [or $D\bar{D}^*$ in the case of the $\chi_{c1}(3872)$ state], it is also a much simpler state from both an experimental and theoretical point of view since the two heavy quarks cannot form a conventional meson. It thus provides better prospects for understanding the relative roles of compact tetraquark and molecular configurations.

The full potential of the already-accumulated LHCb data has not yet been realized. More experimentally difficult final states, including neutral particles ($\gamma, \pi^0, \eta, \omega$), are being analyzed, and results should become available in the coming years. Prompt production of exotic hadrons, which comes with difficult-to-control high backgrounds, may also lead to interesting new observations. Central (semi)exclusive production of clean low-multiplicity final states also has the potential to be fully explored.

To conclude this article, it became very clear from the LHCb discoveries of several narrow pentaquarks near the baryon–meson mass thresholds with heavy quarks inside that a molecular type of binding is at work. More such states are likely to be discovered in the future. This fits well with the narrow heavy-tetraquark states discovered earlier at the e^+e^- colliders near meson–meson thresholds. There are many other observations of broader exotic hadron structures that do not fit the molecular model, which point to the presence of compact color bindings. However, because of the experimental difficulties of resolving broader states as well as the large theoretical uncertainties in modeling such systems, it is harder to draw strong conclusions. It is also quite possible that both types of bindings contribute simultaneously to the formation of the observed structures. More effort is needed on both the experimental and theoretical sides to clarify whether compact multiquark hadrons really exist and how the two types of binding interplay with each other. The order-of-magnitude increase in the data samples expected to be collected using the upgraded LHCb experiment over the next decade, and the further order-of-magnitude increase expected after Upgrade II of the LHCb detector (Section 9), will help toward this goal.

DISCLOSURE STATEMENT

The authors are not aware of any affiliations, memberships, funding, or financial holdings that might be perceived as affecting the objectivity of this review.

ACKNOWLEDGMENTS

This work was supported by the US National Science Foundation (award 2102879), the UK Science and Technology Facilities Council (grant ST/W004305/1), and the 2022/2023 Istituto Nazionale di Fisica Nucleare (INFN) Research Grant Program (announcement 23591).

LITERATURE CITED

1. Gell-Mann M. *Phys. Lett.* 8:214 (1964); Zweig G. Report 8182/TH-401, CERN, Geneva (1964); Zweig G. Report 8419/TH-412, CERN, Geneva (1964)
2. Aaij R, et al. (LHCb Collab.) *Int. J. Mod. Phys. A* 30:1530022 (2015)
3. Archilli F, et al. *J. Instrum.* 8:P10020 (2013)
4. Choi SK, et al. *Phys. Rev. Lett.* 91:262001 (2003)
5. Aubert B, et al. (BaBar Collab.) *Phys. Rev. D* 71:071103 (2005)
6. Acosta D, et al. (CDF II Collab.) *Phys. Rev. Lett.* 93:072001 (2004)
7. Abazov VM, et al. (D0 Collab.) *Phys. Rev. Lett.* 93:162002 (2004)
8. Aaij R, et al. (LHCb Collab.) *Eur. Phys. J. C* 72:1972 (2012)
9. Abulencia A, et al. (CDF Collab.) *Phys. Rev. Lett.* 98:132002 (2007)
10. Choi SK, et al. (Belle Collab.) *Phys. Rev. D* 84:052004 (2011)
11. Aaij R, et al. (LHCb Collab.) *Phys. Rev. Lett.* 110:222001 (2013)
12. Aaij R, et al. (LHCb Collab.) *Phys. Rev. D* 92:011102 (2015)
13. Aaij R, et al. (LHCb Collab.) *Phys. Rev. D* 108:L011103 (2023)
14. Tornqvist NA. arXiv:hep-ph/0308277 (2003); Tornqvist NA. *Phys. Lett. B* 590:209 (2004); Voloshin MB. *Phys. Lett. B* 579:316 (2004); Swanson ES. *Phys. Lett. B* 588:189 (2004)
15. Terasaki K. *Prog. Theor. Phys.* 118:821 (2007); Maiani L, Polosa AD, Riquer V. *Phys. Lett. B* 778:247 (2018)
16. Aaij R, et al. (LHCb Collab.) *J. High Energy Phys.* 2008:123 (2020)
17. Aaij R, et al. (LHCb Collab.) *Phys. Rev. D* 102:092005 (2020)
18. Workman RL, et al. (Part. Data Group.) *PTEP* 2022:083C01 (2022)
19. Aubert B, et al. (BaBar Collab.) *Phys. Rev. Lett.* 102:132001 (2009)
20. Bhardwaj V, et al. (Belle Collab.) *Phys. Rev. Lett.* 107:091803 (2011)

21. Aaij R, et al. (LHCb Collab.) *Nucl. Phys. B* 886:665 (2014)
22. Swanson ES. 2004. In *Proceedings of the 32nd International Conference on High Energy Physics (ICHEP 2004)*, ed. H Chen, D Du, W Li, C Lu, pp. 1037–39. Singapore: World Sci.
23. Dong Y, Faessler A, Gutsche T, Lyubovitskij VE. *J. Phys. G* 38:015001 (2011)
24. Ferretti J, Galatà G, Santopinto E. *Phys. Rev. D* 90:054010 (2014)
25. Guo FK, et al. *Phys. Lett. B* 742:394 (2015)
26. Takeuchi S, Takizawa M, Shimizu K. *JPS Conf. Proc.* 17:112001 (2017)
27. Ablikim M, et al. (BESIII Collab.) *Phys. Rev. Lett.* 124:242001 (2020)
28. Aaij R, et al. (LHCb Collab.) *J. High Energy Phys.* 2102:24 (2021). Erratum. *J. High Energy Phys.* 2104:170 (2021)
29. Aaij R, et al. (LHCb Collab.) *J. High Energy Phys.* 2307:84 (2023)
30. Aaij R, et al. (LHCb Collab.) *J. High Energy Phys.* 1909:28 (2019)
31. Sirunyan AM, et al. (CMS Collab.) *Phys. Rev. Lett.* 125:152001 (2020)
32. Maiani L, Polosa AD, Riquer V. *Phys. Rev. D* 102:034017 (2020)
33. Aaij R, et al. (LHCb Collab.) *J. High Energy Phys.* 2201:131 (2022)
34. Aaij R, et al. (LHCb Collab.) *Phys. Rev. Lett.* 126:092001 (2021)
35. Esposito A, et al. *Eur. Phys. J. C* 81:669 (2021)
36. Braaten E, He LP, Ingles K, Jiang J. *Phys. Rev. D* 103:L071901 (2021)
37. Aaij R, et al. (LHCb Collab.) Report LHCb-CONF-2022-001/CERN-LHCb-CONF-2022-001, CERN, Geneva (2022)
38. Sirunyan AM, et al. (CMS Collab.) *Phys. Rev. Lett.* 128:032001 (2022)
39. Isgur N, Karl G. *Phys. Rev. D* 18:4187 (1978)
40. Nakano T, et al. *Phys. Rev. Lett.* 91:012002 (2003)
41. Stepanyan S, et al. (CLAS Collab.) *Phys. Rev. Lett.* 91:252001 (2003)
42. Kubarovsky V, et al. (CLAS Collab.) *Phys. Rev. Lett.* 92:032001 (2004). Erratum. *Phys. Rev. Lett.* 92:049902 (2004)
43. Aaij R, et al. (LHCb Collab.) *Phys. Rev. Lett.* 115:072001 (2015)
44. Aaij R, et al. (LHCb Collab.) *Phys. Rev. Lett.* 122:222001 (2019)
45. Aaij R, et al. (LHCb Collab.) *Sci. Bull.* 66:1278 (2021)
46. Aaij R, et al. (LHCb Collab.) *Phys. Rev. Lett.* 128:062001 (2022)
47. Aaij R, et al. (LHCb Collab.) *Phys. Rev. Lett.* 131:031901 (2023)
48. Aaij R, et al. (LHCb Collab.) *Phys. Rev. Lett.* 117:082002 (2016)
49. Wang M, et al. *Chin. Phys. C* 45:063103 (2021)
50. Ali A, Parkhomenko AY. *Phys. Lett. B* 793:365 (2019)
51. Liu MZ, et al. *Phys. Rev. Lett.* 122:242001 (2019)
52. Yang ZC, et al. *Chin. Phys. C* 36:6 (2012)
53. Wu JJ, Molina R, Oset E, Zou BS. *Phys. Rev. Lett.* 105:232001 (2010)
54. Wu JJ, Lee TSH, Zou BS. *Phys. Rev. C* 85:044002 (2012)
55. Karliner M, Rosner JL. *Phys. Rev. Lett.* 115:122001 (2015)
56. Chen R, Sun ZF, Liu X, Zhu SL. *Phys. Rev. D* 100:011502 (2019)
57. Guo FK, Jing HJ, Meißner UG, Sakai S. *Phys. Rev. D* 99:091501 (2019)
58. He J. *Eur. Phys. J. C* 79:393 (2019)
59. Huang H, He J, Ping J. arXiv:1904.00221 [hep-ph] (2019)
60. Shimizu Y, Yamaguchi Y, Harada M. arXiv:1904.00587 [hep-ph] (2019)
61. Guo ZH, Oller JA. *Phys. Lett. B* 793:144 (2019)
62. Xiao CJ, et al. *Phys. Rev. D* 100:014022 (2019)
63. Meng L, Wang B, Wang GJ, Zhu SL. *Phys. Rev. D* 100:014031 (2019)
64. Wu Q, Chen DY. *Phys. Rev. D* 100:114002 (2019)
65. Shen CW, Wu JJ, Zou BS. *Phys. Rev. D* 100:056006 (2019)
66. Xiao CW, Nieves J, Oset E. *Phys. Lett. B* 799:135051 (2019)
67. Voloshin MB. *Phys. Rev. D* 100:034020 (2019)
68. Sakai S, Jing HJ, Guo FK. *Phys. Rev. D* 100:074007 (2019)

69. Wang ZG, Wang X. *Chin. Phys. C* 44:103102 (2020)
70. Yamaguchi Y, et al. *Phys. Rev. D* 101:091502 (2020)
71. Xu YJ, Cui CY, Liu YL, Huang MQ. *Phys. Rev. D* 102:034028 (2020)
72. Pavon Valderrama M. *Phys. Rev. D* 100:094028 (2019)
73. Peng FZ, et al. *Nucl. Phys. B* 983:115936 (2022)
74. Liu MZ, et al. *Phys. Rev. D* 103:054004 (2021)
75. Pan YW, et al. *Phys. Rev. D* 102:011504 (2020)
76. Burns TJ, Swanson ES. *Phys. Rev. D* 100:114033 (2019)
77. Guo FK, Meißner UG, Wang W, Yang Z. *Phys. Rev. D* 92:071502 (2015)
78. Meißner UG, Oller JA. *Phys. Lett. B* 751:59 (2015)
79. Liu XH, Wang Q, Zhao Q. *Phys. Lett. B* 757:231 (2016)
80. Mikhasenko M. arXiv:1507.06552 [hep-ph] (2015)
81. Eides MI, Petrov VY, Polyakov MV. *Mod. Phys. Lett. A* 35:2050151 (2020)
82. Wang M. *Amplitude analysis of the* $\Lambda_b^0 \to J/\psi p K^-$ *decay and first observation of the* $\Lambda_b^0 \to \eta_c(1S) p K^-$ *decay*. PhD Thesis, Tsinghua Univ., Beijing (2021)
83. Aaij R, et al. (LHCb Collab.) *Phys. Rev. Lett.* 117:082003 (2016). Addendum. *Phys. Rev. Lett.* 117:109902 (2016)
84. Aaij R, et al. (LHCb Collab.) *Phys. Rev. Lett.* 122:191804 (2019)
85. Hsiao YK, Geng CQ. *Eur. Phys. J. C* 75:101 (2015)
86. Mikhasenko M, et al. *Phys. Rev. D* 101:034033 (2020)
87. Karliner M, Rosner JL. *Phys. Rev. D* 106:036024 (2022)
88. Choi SK, et al. (Belle Collab.) *Phys. Rev. Lett.* 100:142001 (2008)
89. Aubert B, et al. (BaBar Collab.) *Phys. Rev. D* 79:112001 (2009)
90. Aaij R, et al. (LHCb Collab.) *Phys. Rev. Lett.* 112:222002 (2014)
91. Chilikin K, et al. (Belle Collab.) *Phys. Rev. D* 88:074026 (2013)
92. Chilikin K, et al. (Belle Collab.) *Phys. Rev. D* 90:112009 (2014)
93. Aaij R, et al. (LHCb Collab.) *Phys. Rev. D* 92:112009 (2015)
94. Aaij R, et al. (LHCb Collab.) *Phys. Rev. Lett.* 122:152002 (2019)
95. Beiter A. *Amplitude analysis of* B^0 *decays to* $J/\Psi\pi^- K^+$ *and* $\psi(2S)\pi^- K^+$. PhD Thesis, Syracuse Univ., Syracuse, NY (2023)
96. Aaltonen T, et al. (CDF Collab.) *Phys. Rev. Lett.* 102:242002 (2009)
97. Cheng-Ping S. (Belle Collab.) *Chin. Phys. C* 34:615 (2010)
98. Aaltonen T, et al. (CDF Collab.) *Mod. Phys. Lett. A* 32:1750139 (2017)
99. Aaij R, et al. (LHCb Collab.) *Phys. Rev. D* 85:091103 (2012)
100. Lees JP, et al. (BaBar Collab.) *Phys. Rev. D* 91:012003 (2015)
101. Chatrchyan S, et al. (CMS Collab.) *Phys. Lett. B* 734:261 (2014)
102. Abazov VM, et al. (D0 Collab.) *Phys. Rev. Lett.* 115:232001 (2015)
103. Abazov VM, et al. (D0 Collab.) *Phys. Rev. D* 89:012004 (2014)
104. Aaij R, et al. (LHCb Collab.) *Phys. Rev. D* 95:012002 (2017)
105. Aaij R, et al. (LHCb Collab.) *Phys. Rev. Lett.* 118:022003 (2017)
106. Aaij R, et al. (LHCb Collab.) *Phys. Rev. Lett.* 127:082001 (2021)
107. Aaij R, et al. (LHCb Collab.) *Phys. Rev. Lett.* 131:131901 (2023)
108. Aaij R, et al. (LHCb Collab.) *Phys. Rev. D* 108:034012 (2023)
109. Aaij R, et al. (LHCb Collab.) *Phys. Rev. Lett.* 131:071901 (2023)
110. Molina R, Branz T, Oset E. *Phys. Rev. D* 82:014010 (2010)
111. Liu YR, Liu X, Zhu SL. *Phys. Rev. D* 93:074023 (2016)
112. Cheng JB, et al. *Phys. Rev. D* 101:114017 (2020)
113. Aaij R, et al. (LHCb Collab.) *Phys. Rev. Lett.* 125:242001 (2020)
114. Aaij R, et al. (LHCb Collab.) *Phys. Rev. D* 102:112003 (2020)
115. Burns TJ, Swanson ES. *Phys. Rev. D* 103:014004 (2021)
116. Guo T, Li J, Zhao J, He L. *Phys. Rev. D* 105:054018 (2022)
117. Molina R, Oset E. *Phys. Rev. D* 107:056015 (2023)

118. Liu XH, et al. *Eur. Phys. J. C* 80:1178 (2020)
119. Aaij R, et al. (LHCb Collab.) *Phys. Rev. Lett.* 131:041902 (2023)
120. Aaij R, et al. (LHCb Collab.) *Phys. Rev. D* 108:012017 (2023)
121. Lian DK, et al. *Eur. Phys. J. C* 84:1 (2024)
122. Agaev SS, Azizi K, Sundu H. *Phys. Rev. D* 107:094019 (2023)
123. Dmitrašinović V. arXiv:2301.05471 [hep-ph] (2023)
124. Aaij R, et al. (LHCb Collab.) *Sci. Bull.* 65:1983 (2020)
125. Aaij R, et al. (LHCb Collab.) *J. High Energy Phys.* 1810:86 (2018)
126. Sirunyan AM, et al. (CMS Collab.) *Phys. Lett. B* 808:135578 (2020)
127. Iwasaki Y. *Phys. Rev. Lett.* 36:1266 (1976)
128. Chao KT. *Z. Phys. C* 7:317 (1981)
129. Ader J, Richard J, Taxil P. *Phys. Rev. D* 25:2370 (1982)
130. Li BA, Liu KF. *Phys. Rev. D* 29:426 (1984)
131. Berezhnoy AV, Luchinsky AV, Novoselov AA. *Phys. Rev. D* 86:034004 (2012)
132. Wu J, et al. *Phys. Rev. D* 97:094015 (2018)
133. Karliner M, Nussinov S, Rosner JL. *Phys. Rev. D* 95:034011 (2017)
134. Barnea N, Vijande J, Valcarce A. *Phys. Rev. D* 73:054004 (2006)
135. Debastiani VR, Navarra FS. *Chin. Phys. C* 43:013105 (2019)
136. Liu MS, Lü QF, Zhong XH, Zhao Q. *Phys. Rev. D* 100:016006 (2019)
137. Chen W, et al. *Phys. Lett. B* 773:247 (2017)
138. Wang GJ, Meng L, Zhu SL. *Phys. Rev. D* 100:096013 (2019)
139. Bedolla MA, Ferretti J, Roberts CD, Santopinto E. *Eur. Phys. J. C* 80:1004 (2020)
140. Lloyd RJ, Vary JP. *Phys. Rev. D* 70:014009 (2004)
141. Chen X. arXiv:2001.06755 [hep-ph] (2020)
142. Wang ZG, Di ZY. *Acta Phys. Polon. B* 50:1335 (2019)
143. Anwar MN, et al. arXiv:1710.02540 [hep-ph] (2017)
144. Aad G, et al. (ATLAS Collab.) *Phys. Rev. Lett.* 131:151902 (2023)
145. Hayrapetyan A, et al. (CMS Collab.) arXiv:2306.07164 [hep-ex] (2023)
146. Dong XK, et al. *Phys. Rev. Lett.* 126:132001 (2021). Erratum. *Phys. Rev. Lett.* 127:119901 (2021)
147. Aaij R, et al. (LHCb Collab.) *Phys. Rev. Lett.* 119:112001 (2017)
148. Aaij R, et al. (LHCb Collab.) *J. High Energy Phys.* 2002:49 (2020)
149. Ballot J, Richard J. *Phys. Lett. B* 123:449 (1983)
150. Karliner M, Rosner JL. *Phys. Rev. Lett.* 119:202001 (2017)
151. Aaij R, et al. (LHCb Collab.) *Nat. Phys.* 18:751 (2022)
152. Aaij R, et al. (LHCb Collab.) *Nat. Commun.* 13:3351 (2022)
153. Janc D, Rosina M. *Few Body Syst.* 35:175 (2004)
154. Aaij R, et al. (LHCb Collab.) arXiv:2305.10515 [hep-ex] (2023)
155. Barschel C. *Precision luminosity measurement at LHCb with beam-gas imaging*. PhD Thesis, RWTH Aachen Univ., Aachen, Ger. (2014)
156. LHCb Collab. Report CERN-LHCC-2021-012/LHCB-TDR-023, CERN, Geneva (2021)
157. Lebed RF, et al. arXiv:2207.14594 [hep-ph] (2022)